ARL-TR-7271 ● Apr 2015

US Army Research Laboratory

Level-Dependent Nonlinear Hearing Protector Model in the Auditory Hazard Assessment Algorithm for Humans

by Paul Fedele and Joel Kalb

NOTICES

Disclaimers

The findings in this report are not to be construed as an official Department of the Army position unless so designated by other authorized documents.

Citation of manufacturer's or trade names does not constitute an official endorsement or approval of the use thereof.

Destroy this report when it is no longer needed. Do not return it to the originator.

ARL-TR-7271 ● APR 2015

US Army Research Laboratory

Level-Dependent Nonlinear Hearing Protector Model in the Auditory Hazard Assessment Algorithm for Humans

by Paul Fedele and Joel Kalb
Human Research and Engineering Directorate, ARL

REPORT DOCUMENTATION PAGE

Form Approved
OMB No. 0704-0188

1. REPORT DATE *(DD-MM-YYYY)*	2. REPORT TYPE	3. DATES COVERED (From - To)
April 2015	Final	1 October 2013–31 October 2014

4. TITLE AND SUBTITLE
Level-Dependent Nonlinear Hearing Protector Model in the Auditory Hazard Assessment Algorithm for Humans

5a. CONTRACT NUMBER

5b. GRANT NUMBER

5c. PROGRAM ELEMENT NUMBER

6. AUTHOR(S)
Paul Fedele and Joel Kalb

5d. PROJECT NUMBER

5e. TASK NUMBER

5f. WORK UNIT NUMBER

7. PERFORMING ORGANIZATION NAME(S) AND ADDRESS(ES)
US Army Research Laboratory
ATTN: RDRL-HRS-D
Aberdeen Proving Ground, MD 21005-5425

8. PERFORMING ORGANIZATION REPORT NUMBER
ARL-TR-7271

9. SPONSORING/MONITORING AGENCY NAME(S) AND ADDRESS(ES)

10. SPONSOR/MONITOR'S ACRONYM(S)

11. SPONSOR/MONITOR'S REPORT NUMBER(S)

12. DISTRIBUTION/AVAILABILITY STATEMENT
Approved for public release; distribution is unlimited.

13. SUPPLEMENTARY NOTES

14. ABSTRACT
US Army Research Laboratory technical report ARL-TR-6748, "Using the Auditory Hazard Assessment Algorithm for Humans (AHAAH) With Hearing Protection Software, Release MIL-STD-1474E," includes AHAAH with a Hearing Protector Module (HPM) modeling all hearing protector devices (HPDs) as level-independent linear devices. Listed HPDs include several level-dependent nonlinear (LDNL) earplugs. These are modeled linearly, based on Real Ear Attenuation at Threshold (REAT) measurements in closed and open modes. When analyzing auditory hazards with LDNL HPDs applied as linear devices based on REAT measurements, results are generally overly protective, since REAT measurements do not reflect increased attenuations for higher waveform pressures. Several MIL-STD-1474E Working Group members felt LDNL HPD performance must be accurately described and incorporated into AHAAH cited in the MIL-STD. Consequently, a nonlinear pressure-amplitude-dependent model for performance of LDNL HPDs was created and added to the HPM of version 2.1 of AHAAH (Release MIL-STD-1474E). We describe LDNL modifications to AHAAH's HPM and validate the LDNL HPD model by comparing predicted and measured insertion losses (ILs) and waveforms under the HPD, for increasingly intense waveforms. A LDNL HPM will more accurately predict ILs and waveforms under HPDs and support more accurate auditory hazard assessments for complex impulsive waveforms encountered in real situations.

15. SUBJECT TERMS
Impulsive noise, hearing protector, nonlinear, AHAAH, amplitude and time-scale dependence

16. SECURITY CLASSIFICATION OF:			17. LIMITATION OF ABSTRACT	18. NUMBER OF PAGES	19a. NAME OF RESPONSIBLE PERSON
a. REPORT	b. ABSTRACT	c. THIS PAGE			Paul Fedele
Unclassified	Unclassified	Unclassified	UU	66	19b. TELEPHONE NUMBER (Include area code) 410-278-5984

Contents

List of Figures

INTENTIONALLY LEFT BLANK

1. Introduction

The Auditory Hazard Assessment Algorithm for Humans (AHAAH) (http://www.arl.army.mil/www/default.cfm?page=343) is an advance in the evaluation of hearing damage risk associated with impulsive noise. AHAAH applies pressure response dynamics measured for the external, middle, and inner ear to biomechanically model the ear's physical response and accurately determine the strain-induced fatigue occurring in the cochlea's organ of Corti. Instructions for using AHAAH also are available at the US Army Research Laboratory website (Fedele et al. 2013).

AHAAH is based on many decades of research on hearing processes. AHAAH's middle ear dynamics model and basilar membrane strain damage model are consistent with previous testing (Price 1979, 1981, 1983, and Price et al. 1989), and the overall AHAAH model is validated by its ability to reproduce the observations of human trials (Price 2007). At stimulus levels above 135 dB, nonlinear stapes displacement observed in animals by Guinan and Peake (1967) forms the basis of a peak-clipping nonlinearity applied in AHAAH. AHAAH also is consistent with stapes rocking motion observed in human cadavers, as reported by Guelke and Keen (1952). Motion of the cochlea was observed by Bekesy (1955) and later more fully detailed by Bekesy (1960). Aural reflex introduces adaptive changes to the middle ear, which have been both observed and modeled by Lutman and Martin (1979). Physiological damage and associated behavior changes consistent with AHAAH predictions have been observed after exposure to impulsive stimuli, as reported by Price (1979), Dancer, Grateau, Cabanis, Lejau, et al., (1991), Dancer, Grateau, Cabanis, Vaillant, et al., (1991), Hamernik et al. (1991), and Patterson et al.(1993).

As impulsive stimulus peak levels exceed 140 dB, most damage risk criteria consider exposures to be hazardous and require the use of hearing protective devices (HPDs). It is widely observed that properly worn HPDs give complete protection (Berger 2005), and considerable effort has gone into measuring pressure under the HPDs worn by humans (Dancer et al. 1992; Johnson 1993) and manikins (Hamery and Dancer 1999; Parmentier et al. 2000; Dancer et al. 2003; and Buck 2009).

While several damage models, including the LAeq8hr-based analyses, can analyze hearing damage risk from waveforms measured under HPDs, energy-based analyses offer no physical explanation why, as shown by Kalb (2015), a low level of energy at the ear canal entrance of a bare ear is hazardous, while a much higher level of energy at the ear canal entrance of a muff-covered ear is not hazardous.

AHAAH eliminates such inconsistencies by accurately analyzing the pressure-time dependence of the wave at the ear canal entrance. The wave outside the bare ear may have lower energy than the wave outside the muff-covered ear, but it also has a different pressure-time dependence than the higher energy than the wave outside muff-covered ear. Because of the nonlinear characteristics of the middle ear, the bare-ear wave transfers energy through the middle ear much more efficiently than the muff-covered wave. With AHAAH, there is no unexplainable empirical process that makes certain lower energy waves more damaging than higher energy waves; there is only physical dynamics of nonlinear behavior in stretching ligaments.

Overall, although alternate forms of damage models have been proposed, no proposed analysis processes other than AHAAH have been validated against impulsive sounds with a wide range of peak pressures and time-behaviors. The inadequacy of linearly applied analyses based on goo has been clearly shown by Henderson and Hamernik, (1986), while Patterson et al. (1986) has shown failure of peak pressure and total energy to consistently describe auditory damage. Methods that use summary waveform characteristics, such as total A-weighted energy or positive pulse duration, to adjust allowed levels of LAeq8hr may prove accurate for a narrow range of waveform variations, such as waveforms limited to classical Friedlanders with varying peak pressures; However, a full account of all major nonlinear transmission characteristics is necessary to accurately assess hearing protector performance and ear response to arbitrary impulsive waveforms.

AHAAH's nonlinear middle ear transmission characteristics and the nonlinear behavior of hearing protectors allow AHAAH to more accurately evaluate hearing damage risk over a wider range of waveform variations. With the new addition of a level-dependent nonlinear (LDNL) HPD, AHAAH is able to address LDNL HPD performance against measured free-field waveforms and provide hearing damage assessments, which also account for nonlinear middle ear transmission.

2. Linear Hearing Protection Model

Before describing AHAAH's LDNL HPD model, we first review AHAAH's level-independent linear (LIL) HPD model.

In an article on measuring HPD attenuation, Berger (1986) points out that Real Ear Attenuation at Threshold (REAT) tests are typically below 60 decibels (dB) sound pressure level (SPL) and asks if this accurately represents HPD attenuation at higher sound levels. He finds "for intentionally linear protectors, i.e., not containing valves, orifices, thin diaphragms, or active circuitry, attenuation appears to be independent of SPL up to very-high sound levels. Therefore, REAT test results can be assumed to be indicative of performance in high-level-noise environments".

Berger's observations provide a basis for applying REAT measurements, as a beginning in characterizing all hearing protector performance. He goes on to qualify this statement for impulsive noise: "Whether or not the response of intentionally nonlinear HPDs to gunfire and cannon impulses, blasts, and explosions is accurately represented by an REAT test is open to question". At the time, this qualification appears more for the earmuffs than earplugs, but currently, our measurements, and those of others, show intentionally nonlinear hearing protectors, and hearing protectors with various protrusions, do require added evaluations against a wider range of impulsive waveforms, if we intend to characterize the full protection that these devises offer.

As described by Kalb (2013), LIL hearing protector performance can be described by a 3-piston model. The 3-piston model consists of a leak piston, a whole-hearing-protector piston, and a hearing-protector material deformation piston. Each of these model components is briefly described in the following paragraphs.

The leak piston represents a volume of air that moves as a single unit under the influence of pressure differences across it. The leak piston has no inherent restoring force associated with its displacement; its movement depends only on resistance to viscous and turbulent flow and the pressure difference across the leak path, in general the difference between the pressure outside the hearing protector and the pressure under the hearing protector.

The whole-hearing-protector piston represents movement of a rigid representation of the entire hearing protector under the pressure difference across it. Unlike the leak piston, the whole hearing protector piston has a restoring force dependent on its displacement. In the case of an ear muff, this force represents the response to combined compression of ear-cushion foam and the skin about the ear. With an ear plug, this force represents the flexing of the earplug material and the skin holding the earplug in the ear canal.

Last, the material deformation piston represents flexing of the hearing protector itself, apart from net displacement, which has already been associated with movement of the whole hearing protector as a single rigid-body piston. This path represents the next higher mode of vibration of the hearing protector. In a simple geometry, material deformation movement can occur at a frequency near double the frequency of movement of the whole hearing protector as a rigid body, but in more complex geometries deformation movement can vary. The model applies a material deformation path, adjusts the path's parameters to fit measured insertion loss, and use the application to model transmissions caused by other waveforms.

Various examples given by Kalb (2013) demonstrate the ability of the 3-piston model to describe the performance of liner hearing protectors. Although the 3-piston model does not guarantee fit to all possible hearing protectors, the model fits existing hearing protector REAT measurements. Thus, the validity of this model is established by the model's ability to fit existing HPD performance measurements in general and by its ability to predict pressure wave forms under these hearing protectors (Kalb 2013).

The acoustic performance of the 3-piston model is calculated using the electro-acoustic analogy that is routinely applied in acoustical engineering. The electro-acoustic analogy is a standard analytical technique used the field of acoustics (Olsen 1957). The 3-piston linear hearing protection model is illustrated by electro-acoustic analogy in Fig. 1 (Kalb 2013).

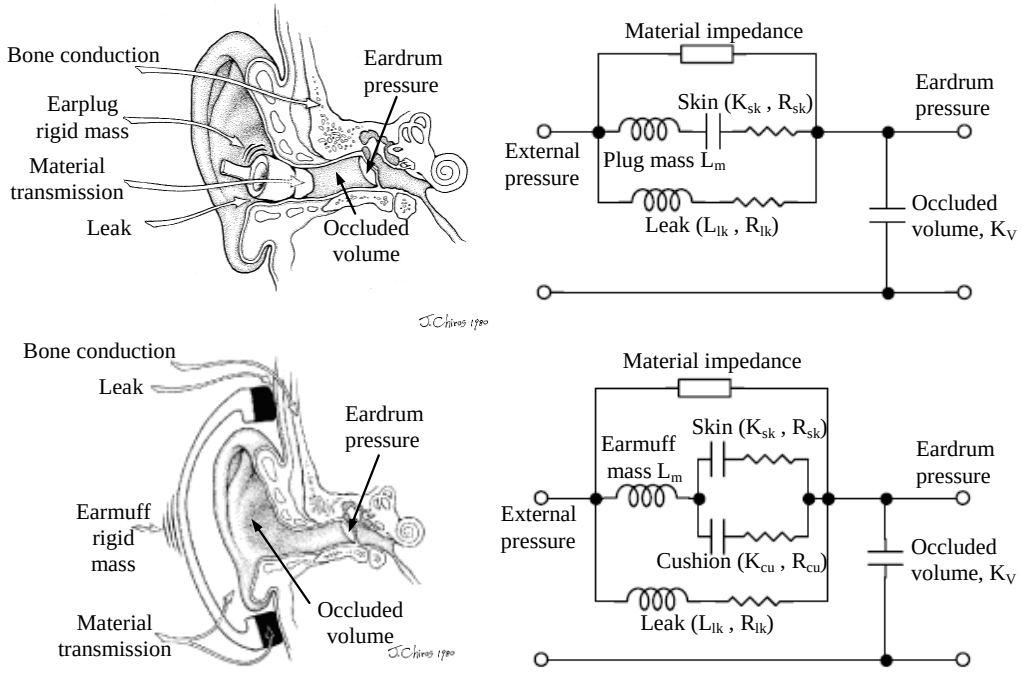

Fig. 1 Electro-acoustic representations of the 3-piston hearing protector model for level-independent earplugs (above) and earmuffs (below). (Ear graphic adapted from, and courtesy of, EH Berger, 3M personal Safety Division, St. Paul, MN.)

In the upper earplug model, the 3 pistons are shown along the 3 circuit lines in the upper part of the circuit diagram. The 3 circuit lines are labeled "Material impedance", representing the material deformation piston shown as the top circuit line, "Plug mass and Skin", representing the whole-hearing-protector piston shown as the middle circuit line, and "Leak", representing the leak piston on the lower circuit line. The lower earmuff model contains the same labeled parameters as the

earplug model, with the addition of a cushion that acts in parallel with the skin in the whole-hearing-protector piston middle circuit line. In the mechanical HPD system, a parallel arrangement of the mechanical springs (capacitors) and mechanical shock absorbers (resistors) means that the velocity of the earmuff mass equals the sum of the velocities of the skin and supporting cushion.

The elements in Fig. 1 are described as follows: Elements represented by a capital "L", are electrical inductors. Inductors act to resist changes in electric current flow rate. This action is analogous to the action of mass in a mechanical system. It accounts for inertia in the movement of each hearing protector piston. Elements represented by a capital "R" are electrical resistors. When electric current moves through the resistor, energy is dissipated and removed from transmission. It does not matter which direction the current is moving; energy is lost by current movement in either direction. That energy is not recovered and it is not transferred to the next part of the system. In a mechanical system, this action is like a shock-absorber. It resists movement in either direction, and converts some of the movement energy into heat, which is lost to the dynamic motion of the system. Elements represented by a capital "K" are the stiffness coefficients of mechanical springs, which are analogous to electrical capacitors. A capacitor becomes charged when a voltage induces a current flow into the capacitor, and the capacitor will discharge (spring back) when the applied voltage decreases. This action is like a spring in a mechanical system. The spring becomes compressed when a force is applied causing a displacement that shortens its length, and it will spring back when the applied force decreases. The leak path does not contain its own specific capacitor, or analogously, mechanical spring. This air piston derives its restoring force only from the increase in pressure in the entire volume occluded by the hearing protector, which is represented by the capacitor labeled "Occluded volume". To avoid clutter, the elements in the material impedance path are not illustrated. This path was noted by Zwislocki (1957) as required for additional energy transmission. Shaw and Thiessen (1958) noted the possibility of "multimodal" vibrations within the material of the HPD, while Kalb (2013) refined the process with precisely defined electro-acoustic components representing the dominant mode of vibrational deformation of the HPD materials. This full circuit is shown in Fig. 2.

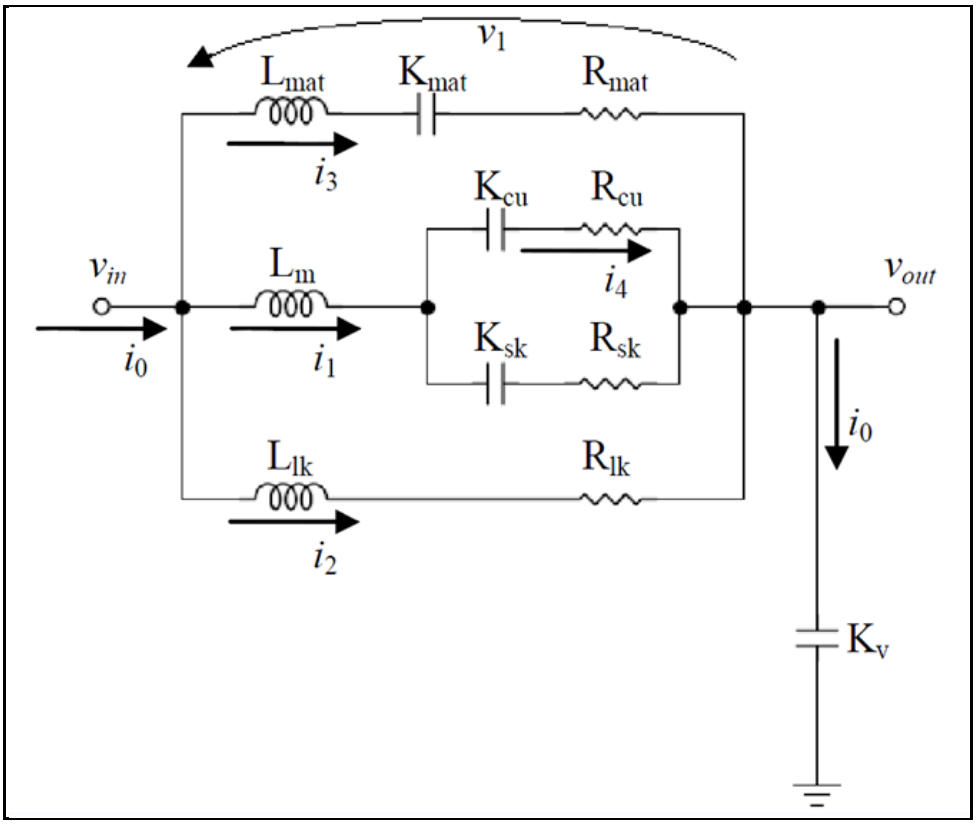

Fig. 2 Electro-acoustic model of the linear 3-piston hearing protector labeling all linear electro-acoustic component values

This material path also contains an inertial inductor, a spring-constant capacitor, and an energy absorbing resistor. As mentioned earlier, the application of electro-acoustics is a standard analytical technique; a detailed description of electro-acoustic-mechanical analogies is given by Olsen (1943), and the analytical techniques have been integrated into the field of acoustical engineering at least since 1957 (Olsen 1957).

The motion of no single piston in the 3-piston model necessarily represents the exact motion of the hearing protector. This is analogous to the way a taught string, which is vibrating between 2 fixed ends, need not move precisely like a finite summation of sine functions (Kreyszig 1972). Rather, these 3 pistons represent movements of 3 low-frequency, independent modes of motion for the hearing protector system, just as the fundamental mode and first 2 overtone modes can combine to represent many possible movements of a vibrating string.

The adequacy with which these 3 modes represent the overall performance of a hearing protector requires empirical justification. The adequacy of the model's representation of a HPD is established when the constant parameters of this 3-piston

model are adjusted to adequately reproduce measured HPD performance. Kalb (2013) demonstrates that the 3-piston model adequately represents many real LIL HPDs.

3. Level-Dependent Nonlinear Modifications to the Linear Model

Linear hearing protectors provide the same frequency-dependent waveform attenuation regardless of the amplitude of the frequency components of the waveform. In many military environments where impulsive noise is encountered, people need to hear low-amplitude sounds, and they also need protection against intermittent high-amplitude impulsive sounds. For Soldiers in battle, many operational advantages are provided by a hearing protector that strongly attenuates high-amplitude waveforms and only limitedly attenuates low-amplitude waveforms. This capability can be achieved with a LDNL HPD. By "level-dependent", we refer to a hearing protector that increases attenuation when waveform pressure increases.

Several hearing protector manufacturers produce hearing protectors offering LDNL performance. Examples of these LDNL HPDs are shown in Figs. 3–7.

Figure 3 shows the metal orifice held used in the plastic, single-flange body of the Gunfender earplug. The Gunfender is a modification of the V-51R earplug shown in Fig. 4.

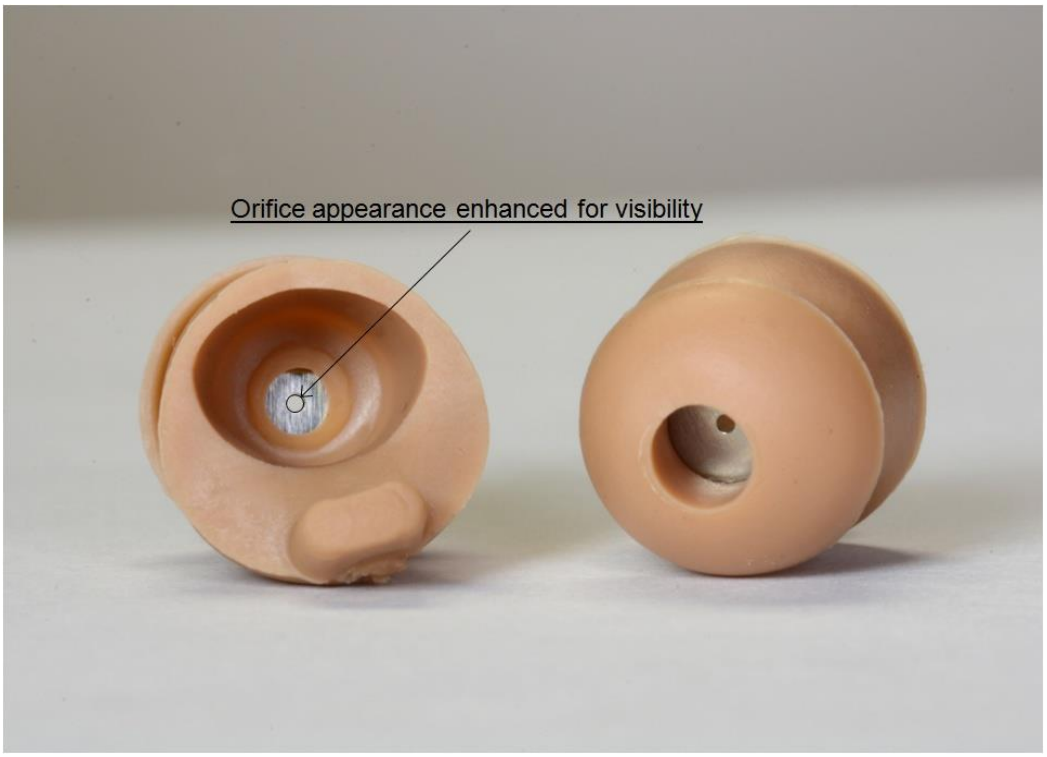

Fig. 3 The Gunfender earplug

Fig. 4 The V-51R; predecessor to the Gunfender

Figure 5 shows the combat arms earplug (CAE) with an orifice visible in the center of the black-plastic insert seen at the end of the white cylinder. This earplug uses a dual orifice design; the black-plastic piece is a hollow cylinder, with an orifice in each end. Sound enters the earplug through the hole seen on the right side of the wider portion of the white cylinder. A yellow earpiece (as shown in Fig. 6) fits over the end of the white cylinder, and sound enters to the eardrum through the hole seen in the end of the yellow earpiece. When turned around with the green end inserted into the ear, no orifice is present and no hole occurs in the inserted end of the earplug. By simply turning the earplug around, the earplug can be switched between the open and the closed configuration.

Fig. 5 Dual-ended combat arms earplug; showing open orifice

Fig. 6 Dual-ended combat arms earplug; showing closed orifice

Figure 7 shows the Quick Response Initiative (QRI) CAE selector dial. The dual-ended design of the CAE dual-ended HPD was replaced by a rotating selector dial. Placing the hole in the selector dial closest to the earpiece opens a path to a dual orifice located in the shaft of the earpiece, creating an open configuration; rotating the hole away from the earpiece closes the path, providing a closed configuration.

Fig. 7 Quick response initiative combat arms earplug; selector dial

Note: Figs. 3–7 Analyzed hearing protectors shown above from the top: Gunfender, V-51R predecessor of the Gunfender, Combat Arms Earplug (CAE) dual ended, and the Quick Response Initiative (CAE) selector dial.

4. A Physics-Based Model of LDNL HPD Performance

Many LDNL HPDs are designed with small orifice openings. The small orifices are designed to remove increasing fractions of energy from increasingly higher pressure impulses. LDNL HPDs do this by inducing vortex shedding from the flow through the orifice and by blocking the transport of shed vortices through the HPD. In principle, as the pressure difference across the orifice increases, more energy is lost to vortices shed at the edges of the orifice, thus removing more energy from the flow. Flow resistance is basically described as the ratio of the pressure drop across the protector to the flow rate through the protector. In linear behavior, the resistance remains constant: the pressure drop across the protector increases linearly with the flow rate through the protector. In level-dependent behavior, the resistance does not remain constant. The resistance increases with the flow rate: the pressure drop across the protector increases faster than linearly with the flow rate through the protector. For example, the resistance may increase by the square of the flow rate.

In Fig. 8, we have plotted acoustic flow resistance measurements for air flow through orifices against flow velocity, as measured by Sivian, (1935). Nonlinearity in the flow resistance is shown when the graph of the resistance in acoustic ohms

(dyne·s·cm^{-5}) versus the flow velocity (cm·s^{-1}) shows that the resistance does not remain constant with changing velocity. Figure 8 clearly shows increasing resistance.

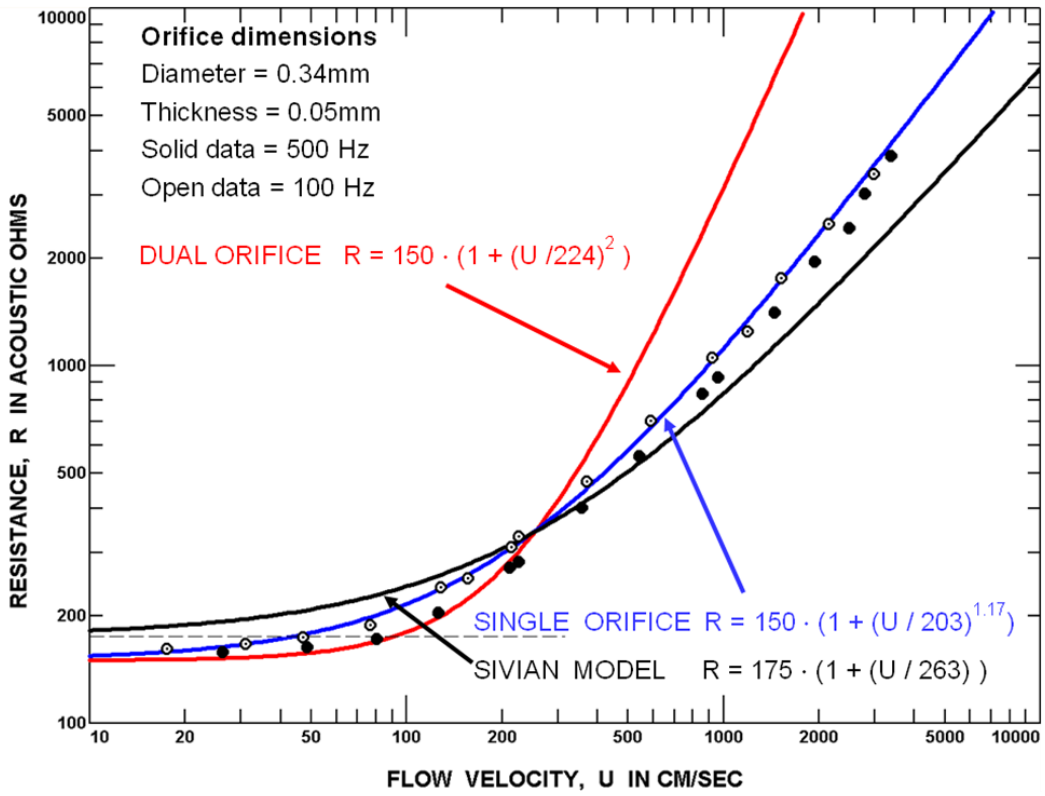

Fig. 8 Resistance of orifice flow plotted vs. flow velocity. Acoustic ohm units are dynes·s·cm^5; the changing resistance demonstrates the process of nonlinear flow through the orifice. (The blue single-orifice fit and the red total resistance for a dual orifice configuration were added by the authors of this report.)

The previously stated orifice resistance measurements show the influence of flow rate on resistance. Rather than a linear dependence where the resistance remains constant with flow rate, the resistance increases with flow rate. The Reynolds number range of data shown in Fig. 8 is 2.4 at 10 cm·s^{-1} to 963 at 4,000 cm·s^{-1}. Marked increases in resistance are seen above a Reynolds number of 240. Sivian used an orifice diameter of 0.34 mm. The CAE orifice diameter is 0.3 mm, and the thickness of the material containing each orifice is comparable. Sivian's fit to the 100- and 500-Hz data is shown by the black curve in Fig. 8, where he approximates the resistance by a linear constant term and a nonlinear turbulence term proportional to the first power of the flow velocity. The equation of this fit is shown in black on the graph. We have applied an alternate fit shown by the blue curve, which depends on a slightly higher power: 1.17, instead of unity.

In Sivian's case a single orifice was used that would be appropriate for simulating the performance of the Gunfender, which has a single orifice through a thin metal plate. Dual orifice resistance is expected to show a higher degree of nonlinearity since the closely coupled second orifice skims the turbulence of flow through the first and also creates its own down-stream turbulence. Nonlinear flow literature shows that Lord Rayleigh (1945) considered a cubic viscous force where the resistance is proportional to the square of the velocity. This level of nonlinearity is shown by the red curve with a velocity-squared dependence. Since both CAEs use dual orifices, the resistance shown by the red curve should apply. The LDNL HPD model calculates the flow using either a resistance that increases linearly with the flow (1-power term) or a resistance that increases with the square of the flow (2-power term). A 1-power or a 2-power term is selected by the variable NL_{Power}. The higher power of the velocity term increases the nonlinear resistance faster than the lower power term, over the velocity range of the nonlinear onset.

Nonlinear electro-acoustic components are added to the linear electro-acoustic representation of the 3-piston HP mode as shown in Fig. 9. Arrows indicate the electro-acoustic component values (EACVs) are no longer contstant. Rather, the EACVs now depend on acoustic displacement or velocity.

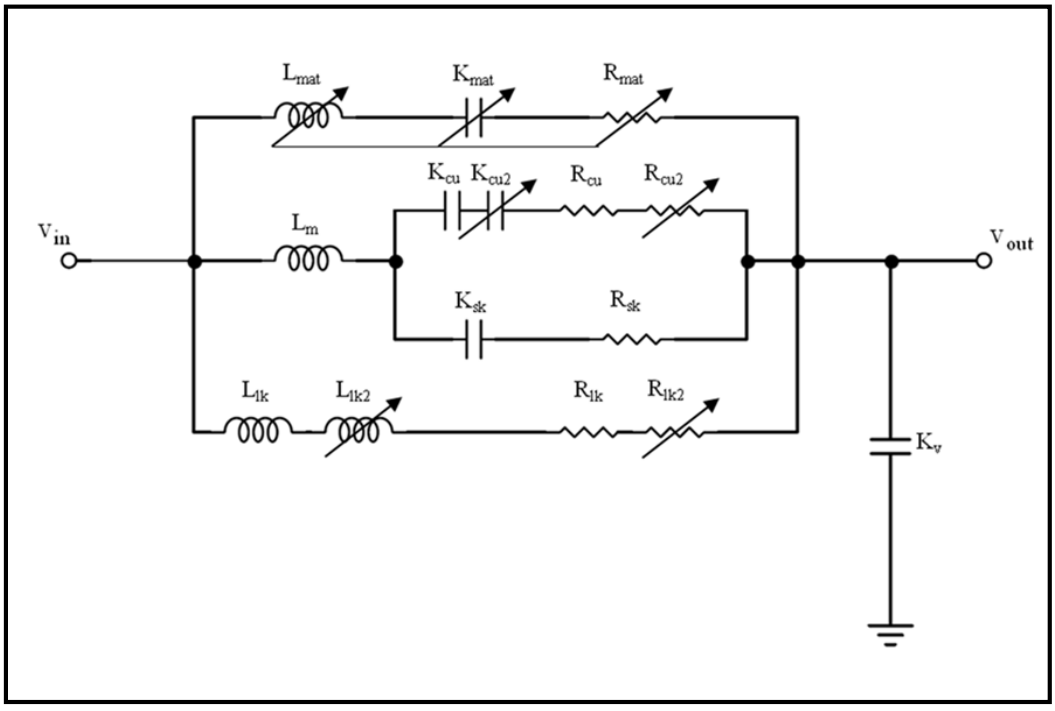

Fig. 9 Schematic diagram of the 3-piston hearing protection model with level-dependent extensions in cushion visco-elastic elements and leakage flow impedance

Consider first the leakage path, shown as the lowest path in Fig. 9. The 2 resistors in series represent the fit to Sivian's data. R_{lk1} is the total acoustic resistance, which equals the sum of the constant linear resistance, R_{lk}, and the added nonlinear resistanec, which equals the product $R_{lk2}.*i_2^2$.

The total resistance is expressed as shown in the following equation:

$$R_{lk1} = R_{lk}\left(1 + R_{lk2} i_2^2\right) = R_{lk}\left(1 + \left(\frac{i_2}{i_{02}}\right)^2\right) \quad R_{lk2} = \left(\frac{1}{i_{02}^2}\right). \tag{1}$$

In Eq. 1, i_2 referrs to the leakage volume velocity ($cm^3 \cdot s^{-1}$) in the EA analogy, and i_{02} is the threshold volume velocity at which the second nonlinear turbulence term has grown to equal the constant linear laminar-flow resistance. The term R_{lk2} represents the coefficient of this nonlinear resistance.

Similarly for the mass of the airplug moving in the leak path

$$L_{lk1} = L_{lk}\left(1 + L_{lk2} i_2^2\right) = L_{lk}\left(1 + \left(\frac{i_2}{i_{02}}\right)^2\right) \quad L_{lk2} = \left(\frac{1}{i_{02}^2}\right). \tag{2}$$

Sivian determined the airplug mass showed no dependence on resistance, so in the second term, $L_{lk2} = 0$. Ingard (1967) on the other hand, showed a dependence on velocity for which the mass could be adjusted. We anticipate that specific tailoring of the edges and contours of the orifice may influence how the effective mass of the leak path piston may change with flow rate. Currently, we apply $L_{lk2} = 0$.

$$K_{mat1} = K_{mat}\left(1 + K_{mat2} i_3^2\right) = K_{mat}\left(1 + \left(\frac{i_3}{i_{03}}\right)^2\right) \quad K_{mat2} = \left(\frac{1}{i_{03}^2}\right). \tag{3}$$

The top circuit represents the secondary piston for modal vibrations in the earplug material. The line connecting all 3 arrows in this path indicates that the values for all 3 circuit elements in this path change together, by means of a common gain factor, K_{mat2}:

$$R_{mat1} = R_{mat} \cdot (1 + K_{mat2}\, i_3^2)\ L_{mat1} = L_{mat} \cdot (1 + K_{mat2}\, i_3^2)\ K_{mat1} = K_{mat} \cdot (1 + K_{mat2}\, i_3^2). \tag{4}$$

These elements are refered to as ganged together. All 3 elements increase with velocity in the same way; they share a common term, K_{mat2}, which is given in the specification of the hearing protector's characteristics (see Eq. 6). This makes the transmission due to this path vary equally at all frequencies maintaining fixed-resonant frequency and quality factor Q.

Last, nonlinear behavior in the movement of the entire HPD as a rigid-body piston is modeled using the value R_{cu2}. Although a corresponding value could as well be added to the resistance of the skin in this path, lacking specific measurements of nonlinear behavior for skin and for earmuff protector foams, we have set to zero all nonlinear terms in the path of the whole HPD as a rigid-body piston.

By selecting values for the parameters i_{02} in the leak path and K_{mat2} in the material path, we establish the nonlinear characteristics of a LDNL HPD.

The equations of motion are given in Fig. 10 (Kalb 2013).

$$
\begin{aligned}
i_0 &= i_1 + i_2 + i_3 \\
v_{out} &= K_v\left(q_1 + q_2 + q_3\right) \\
v_1 &= v_{in} - v_{out} \\
\frac{di_1}{dt} &= \left(v_1 - R_{cu} i_4 - K_{cu} q_4\right) / L_m \\
\frac{di_2}{dt} &= \left(v_1 - R_{lk} i_2\right) / L_{lk} \\
\frac{di_3}{dt} &= \left(v_1 - R_{mat} i_3 - K_{mat} q_3\right) / L_{mat} \\
\frac{di_4}{dt} &= \frac{\left(R_{sk}\frac{di_1}{dt} + K_{sk} i_1 - \left(K_{cu} + K_{sk}\right) i_4\right)}{\left(R_{cu} + R_{sk}\right)}
\end{aligned}
$$

Fig. 10 The set of differential equations describing the 3-piston hearing protector model

In the equations in Fig. 10, *i* refers to electrical current, which is analogus to acoustic volume flow rate, *v* refers to voltage, which is analogus to acoustic pressure, and *q* refers to acoustic flow volume. These equations are identical to the equations for the LIL HPD model given by Kalb (2013), but the coefficients of the current terms (i_1, i_2, i_3 – acoustic volume flow rates) are now functions of the values of the currents themselves, as shown in Eqs. 1–3. The solution of this set of equations does not lend itself to Fourier transform techniques. We solve this set of equations using a Runge-Kutta method of numerical integration (Abramowitz 1964).

5. Comparing Measured Insertion Loss with the LDNL Model's Predictions

The performance of an LDHP can be measured by a series of tests made with an auditory test fixture exposed to impulses with various peak amplitudes and time-dependencies. Auditory test fixtures (ATFs) are manikin head forms instrumented to measure sound pressure at a location corresponding to just outside the eardrum in a human. The result of the variable orifice flow resistance described earlier is to produce waveform attenuation that increases as the pressure amplitude of the waveform increases. The increasing resistance of the orifice flow is seen as an increase in the attenuation of the waveform being transmitted through the hearing protector. The attenuation of transmission through the hearing protector is called insertion loss (IL). IL is calculated as a function of frequency; it is the frequency-dependent amplitude of pressure wave measured at the manikin's simulated eardrum location under the hearing protector divided by the measured frequency-dependent amplitude of the waveform measured at the same manikin location without the hearing protector.

To show that the LDNL HPD model can reproduce measured IL, we demonstrate the model's application to IL measured by Berger and Hamery (2008) for the dual-ended CAE and the Gunfender. Berger and Hamery measured IL using stimulus waveforms with various peak pressure levels in a nonreflective outdoor environment using the ear of the ATF produced by the French-German Institute at Saint-Louis (ISL). This procedure used microphone measurements in an acoustic test fixture (MIATF) taken at grazing incidence on an open dual-ended CAE and on the Gunfender. Test levels ranged from 110 dBP from gunfire to higher levels in 20-dB steps up to 190 dBP. Waveform sources were detonators, primers, and composition-4 (C-4) explosives. Berger and Hamery showed test stimulus waveform spectra typical for Friedlander-type waves at each level. The spectra show peak frequencies, $f_{P,}$ which can be used to approximate the positive phase duration, or A-duration, T_A, of the blast pulses by the relation $T_A = 1/(2\pi f_P)$. Waveforms were measured outside the ear of the ATF and under the HPD.

MIATF measrements cannot be obtained simultaneously both with and without the hearing protector. Further, shot-to-shot variation can cause significant waveform variations that would produce uncertainty in ILs calculated from the sequential MIATF measurements with and without protection. Thus, Berger and Hamery measured the waveform inside the protected ear of the ATF and in the free-field outside the ATF. Using Fourier analysis of the free-field waveform and the predetermined transfer function for the open ear of the ATF, the Fourier components of the free-field waveform were transferred into the open ear of the

ATF. These transferred Fourier components were used to calculate the IL from a single application of the impulsive waveform.

It is well known that the input wave spectral components, when passing through a nonlinear device, generate frequency harmonics and frequency sum and difference components in the output wave. For hearing protectors with nonlinear behavior, attenuation depends on the time-dependent amplitude of the waveform and IL becomes a function of the waveform itself. The transfer function, which gives the ratio of output to input components, is specific to the applied input waveform and can only approximate IL values for waveforms with different amplitudes and time-dependencies. To demonstrate a precise predictive capability for LDNL HPD IL, detailed time-dependent stimulus waveforms must be used.

Berger and Hamery (2008) give the spectra of their stimulus waveforms and indicate the sources used to produce the waveforms. Their waveforms were produced by gunfire at the lowest level (110 dB) and at increasing levels by a detonator (130 dB), a primer (150 dB), or C-4 explosives (170 and 190 dB).They do not give the detailed time-dependent stimulus waveforms needed for application of the LDNL HPD model. However, to compare the LDNL HPD model to their results, we approximated stimulus waveforms using Friedlander waveforms with various appropriately selected positive pressure durations (T_A values) typical of the sources cited.

The time-dependent pressure of a Friedlander waveform, $P_F(t)$, is specified as

$$P_F(t) = P_{peak} e^{-\frac{t}{T_A}} \left(1 - \frac{t}{T_A}\right). \quad (5)$$

In Eq. 5, the time, *t*, starts at zero when the impulse waveform first arrives and continues for positive time, P_{peak} is the peak pressure of the waveform, and T_A marks the time at which the waveform pressure becomes negative, i.e. it is the positive pressure duration of the waveform.

To simulate the stimulus waveforms of a primer or a detonator, we used a Friedlander waveform with a positive pressure duration, T_A, of 0.1 ms, which is typically produced by a rifle cartridge primer. We used a Friedlander with a T_A of 0.3 ms, typical of rifle muzzle blasts measured at the muzzle perpendicular to the line of fire. Further, we compared results obtained with a Friedlander with a 2-ms

T_A, typical of a shoulder-fired recoiless rifle or mortar. Each of these Friedlander waveforms was scaled to the 5 peak positive pressure levels from 110 to 190 dB in 20-dB steps.

By selecting specific values of the LDNL HPD model parameters described previously, we apply the LDNL HPD model with the indicated Friedlander free-field waveforms and compare ILs with those measured by Berger and Hamery (2008) for the dual-ended CAE HPD and the Gunfender.

LDNL HPD model parameters selected for the dual-ended CAE HPD are the following:

$$\begin{aligned} R_{lk2} &= 3{,}100{,}000 \text{ cm}^3.\text{s}^{-1} \\ L_{lk2} &= 0 \text{ g.cm}^{-4} \\ K_{mat2} &= 3.16 \text{ dyne.s}^3.\text{cm}^{-11} \\ K_{cush2} &= 0 \text{ dyne.s}^3.\text{cm}^{-11} \\ NL_{Power} &= 2 \end{aligned} \tag{6}$$

Figures 11–13 show families of IL curves measured for the dual-ended CAE in the ATF developed at ISL. In these figures, the measured IL values are shown in light gray. Each curve is labed with the peak pressure level for which the curve applies. Shown in black are the IL curves predicted by the LDNL HPD model charactrized earlier. These predicted insertion loss values are calculated assuming the pure Friedlander waveform stimuli described earlier.

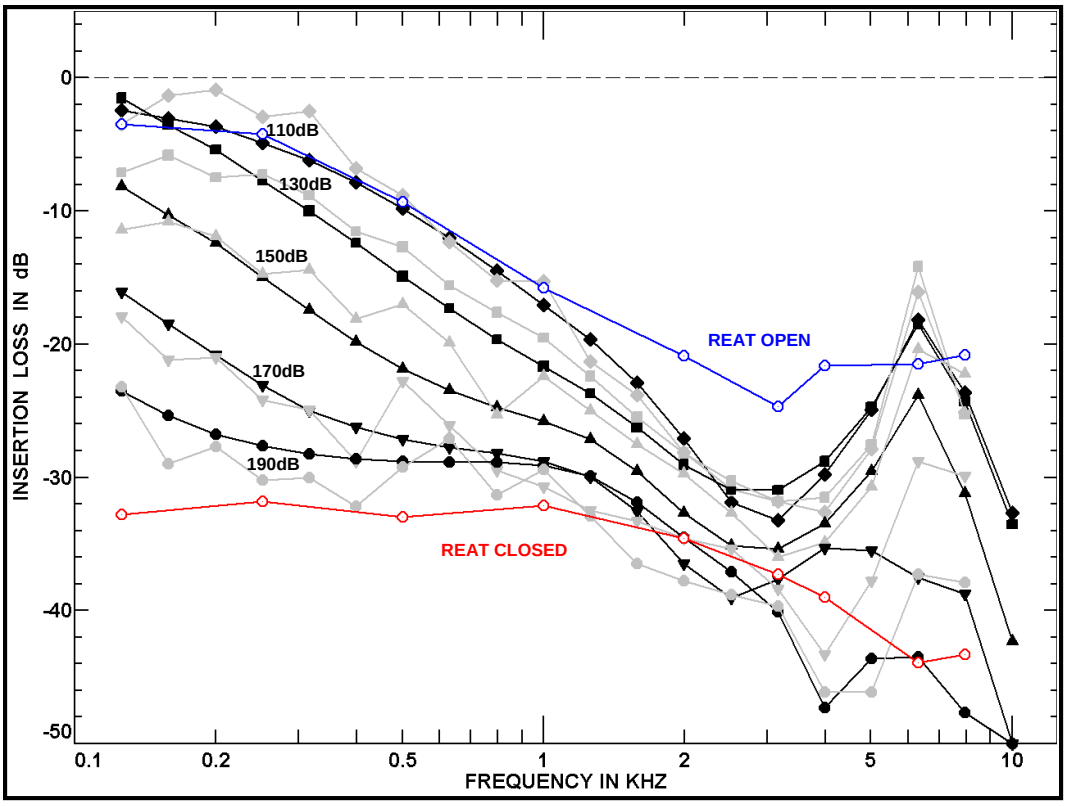

Fig. 11 Dual-ended CAE IL curves in gray measured in ATF for blasts with 110–190 dBP and human derived REAT for closed HPD shown in red and open HPD shown in blue (Berger and Hamery 2008), and LDNL hearing potector model with a stimulus waveform consisting of a 0.1-ms positive pressure duration Friedlander with matching peak pressure levels shown in black.

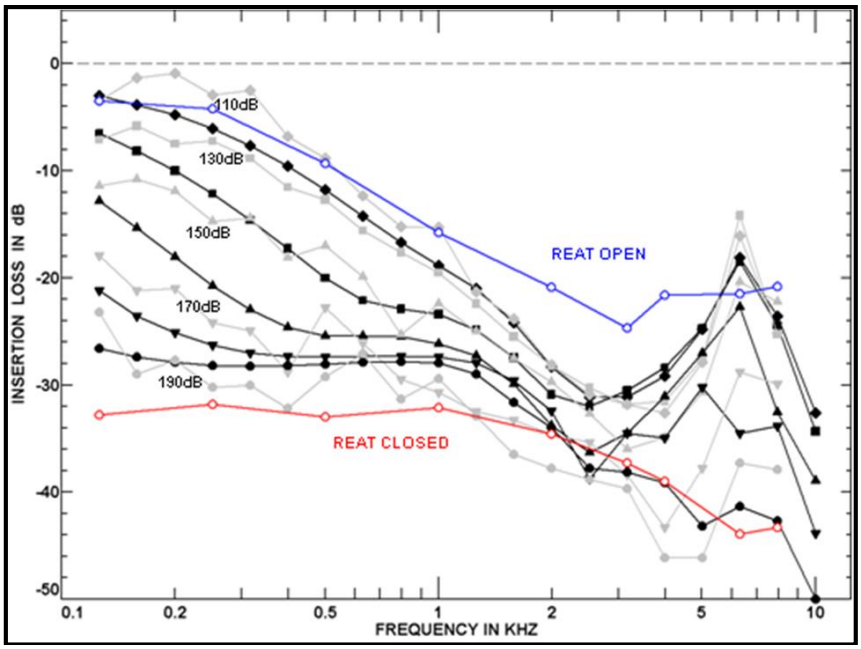

Fig. 12 Dual-ended CAE IL curves in gray measured in ATF for blasts with 110–190 dBP and human derived REAT for closed HPD shown in red and open HPD shown in blue (Berger and Hamery 2008), and LDNL hearing protector model with a Friedlander stimulus waveform with a 0.3-ms positive pressure duration and matching peak pressure levels shown in black.

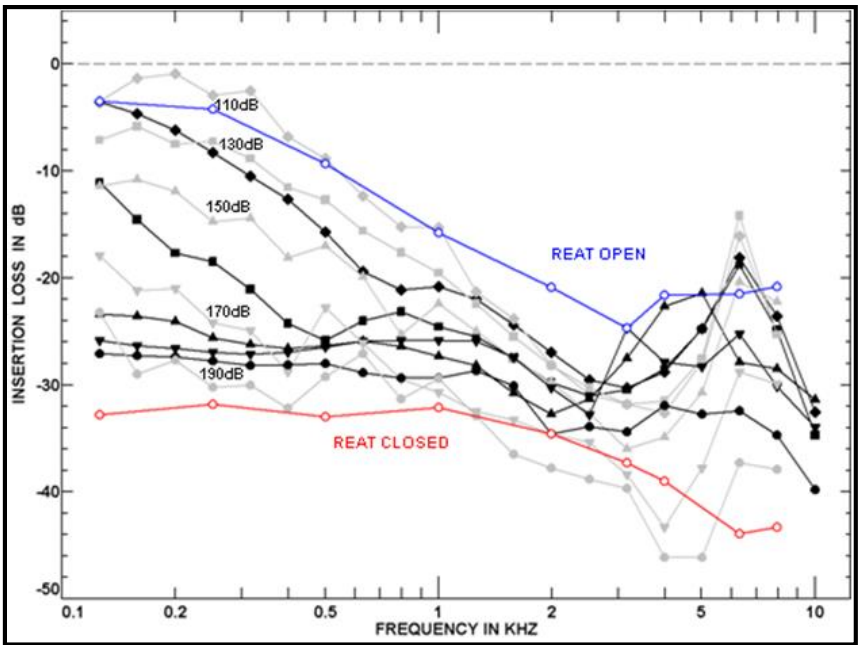

Fig. 13 Dual-ended CAE IL curves in gray measured in ATF for blasts with 110–190 dBP and human derived REAT for closed HPD shown in red and open HPD shown in blue (Berger and Hamery 2008), and LDNL hearing protector model ILs determined from a Friedlander stimulus waveform with a 2.0-ms positive pressure duration and a matching peak pressure level shown in black.

Used in Fig. 11, the Friedlander with a 0.1-ms positive pressure duration simulates a waveform created by a rifle primer blast. The peak of this Friedlander waveform spectrum is 1.6 kHz with energy spectral density level falling at 6 dB/oct above and below this frequency. The predicted IL curves vary consistently with the measurements at each of the 5 peak pressure levels. Figure 11 also shows that the dual-ended CAE shows a resonance at a frequency near 7 kHz that varies with peak pressure level. The measured IL values show a resonance across all amplied waveform peak pressures, with the most pronounced resonance at the lower peak pressures levels. The LDNL HPD model has been parameterized to relect similar resonance behavior. The model characetrization resonance is not as pronounced in the REAT measurements. Since the LDNL HPD model performance at high-peak pressure levels is based on REAT data, the model's resonance is less pronounced for the 190-dBP waveform than for the lower peak pressure waveforms.

The Friedlander used in Fig. 12, with a 0.3-ms duration, simulates a waveform from the muzzle blast of a small-arms rifle. The peak of this waveform spectrum is lowered to 0.53 kHz, which results in some harmonics and intermodulations of the components of the waveform beginning to show at higher frequencies. Overall, the change in stimulus waveform time-dependence has produced a notable but small change in the attenuation. The ILs for the 0.3-ms Friedlander are greater than the attenuations for the 0.1-ms Friedlander, but the differences are small. The change between 0.1 and 0.3 ms appears not to create major variations in LDNL HPD performance.

To examine how the positive phase duration, T_A, of the stimulous waveform influences IL, we assessed IL with the dual-ended CAE using a 2.0-ms duration Friedlander. This waveform approximates the blast produced by a shoulder-fired recoilless rifle or mortar. The peak of this Friedlander stimulus waveform spectrum is now lowered to 0.08 kHz, which allows significant harmonics and intermodulations of the waveform frequency components over the entire frequency analysis range. Figure 13 shows the modeled ILs, again against the background of Berger and Hamery's (2008) measurements.

IL measurements in Figs. 11–13 show a resonance in the dual-ended CAE for frequencies about 6 kHz. This resonance is seen in the measured IL values for all waveform peak pressure levels, but the resonance is not as pronounced in the REAT measurements. Only a few REAT measurements are available in this frequency range, but the REAT measurement at 6.3 kHz does not show the robust resonance behavior seen in the IL measurements. Since REAT measurements are made at peak pressure levels generally well below the lowest peak pressure level used among the stimulus waveforms, the resonance may reflect an amplitude-dependent nonlinear characteristic, but no definite cause of the resonance has been determined. If the

LDNL HPD model is characterized only on the basis of REAT data, the model will not include the full effect of this resonance. In general, the LDNL HPD model can be parameterized to reproduce amplitude-dependent resonant behavior. The LDNL HPD model characterized in Eq. 6 includes an attempt to describe an amplitude-dependent resonance, but no attempt was made to optimize the resonant behavior based on the available measurements.

Compared with Figs. 11 and 12, Fig. 13 shows significant changes in ILs calculated at various peak pressure levels. For the dual-ended CAE HPD, the most IL possible is obtained when the orifice is fully closed, as shown by the red line; the least IL possible is obtained with the orifice opened, as shown by the blue line. ILs are still bounded between the open and closed attenuation levels, but Fig. 13 shows significant increases in IL for the lower peak pressure waveforms with longer durations like the waveforms produced by medium-caliber weapons. Even though the stimulus Friedlander waveforms used with the LDNL HPD model to calculate ILs had the same peak pressures, the waveform's different time dependencies caused considerable differences in ILs.

The 0.1- and 0.3-ms Friedlander waveforms shown in Figs. 11 and 12 provide more likely representations of the measured ILs than the 2.0-ms Friedlander waveforms shown in Fig. 13. As shown in Fig. 11, the 0.1-ms Friedlander produces a good acount of ILs for all frequencies at peak pressure levels. The LDNL HPD model also has been characetrized to display some of the resonance seen in the measurements at frequencies near 6.3 kHz. As noted earlier, the resonance is not as clearly evident in the REAT data for the open or closed earplug. Overall, the applied LDNL parameters allow the modelled IL to transition from levels near the REAT measurements for the open earplug to levels near the REAT measurements for the closed earplug, over a the pressure level range applied in the measrements.

Shown in Fig. 12, the 0.3-ms Friedlander also produces resonance at 6.3 kHz and displays the same decrease in IL values as the peak pressure grows to levels near 190 dB. However, with the 0.3-ms Friedlander, the LDNL HPD model overestimates the IL at lower peak pressure levels. Each black curve generally falls below the coresponding gray curve associated with the same peak pressure level.

Figure 13 gives the least realistic representation of the overall measurements. Although the IL at the highest peak pressure has approached the REAT measurements for the closed earplug, ILs at the lower pressure levels are overestimated. This overestimation of the IL is due to an increased transmision resistance caused because the LDNL flow process occurs over the extended time of the positive pressure pulse of the Friedlander waveform. The frequency spectrum of the 2.0-ms Friedlander waveform occurs at 80 Hz. The peak frequency in the

190-dB waveform applied by Berger and Hamery is at least 100 Hz and may be as high as 400 Hz. The value of 80 Hz is a low estimate for the peak frequency in Berger and Hamery's 190-dB waveform spectrum, so the 2.0-ms Friedlander should result in an overestimate of ILs compared with those measured with Berger and Hamery's 190-dB waveform.

Figures 11, 12, and 13 demonstrate the fundamental aspect of LDNL HPD performance: IL of a LDNL HPD depends not only on the peak pressure or the positive pressure duration but on the full time and amplitude dependence of the stimulus waveform. Thus, IL measurements made with a range of waveforms with various peak pressures may establish IL values for a particular HPD, but those IL measurements apply only to the waveforms used in the measurement. The measured IL values will not accurately apply to stimulus waveforms with other pressure amplitudes. Still further, measured ILs also may not accurately apply to waveforms with different time-dependencies, even when the different waveforms have the same peak pressure. The value of our LDNL HPD model is that by accurately describing physical LDNL process, the model can be used to describe the performance of the HPD against waveforms over a range of amplitudes and time dependencies.

Figure 14 shows Berger and Hamery's grazing incidence measurements of the Gunfender single orifice nonlinear HPD. As noted, the Gunfender HPD was derived from the V-51R single flange passive earplug by the addition of an orifice. Murphy (2014 private communication between Dr William Murphy and Dr Joel Kalb; unreferenced) indicates that the attenuation performance of the V-51R should provide a good representation of the performance of the Gunfender if the Gunfender had a closed configuration because the Gunfender originated as a V-51R with an added orifice.

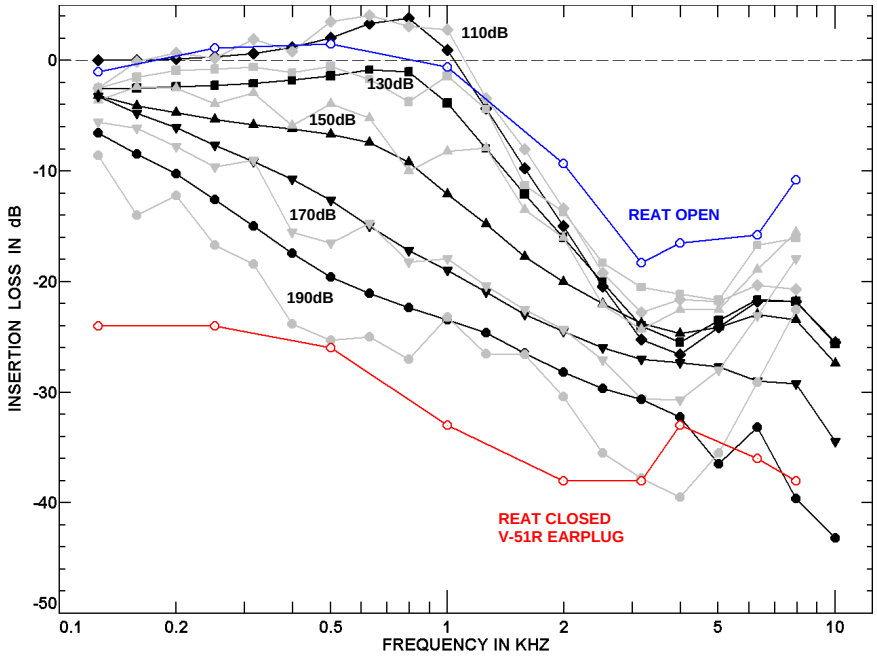

Fig. 14 Gunfender IL curves are shown in gray, as measured in an ATF using blasts with 110–190 dB peak pressure levels. Human derived REAT measurements for the closed V-51R predecessor HPD are shown in red and REAT measurements for the open Gunfender are shown in blue. Shown in black are ILs calculated using the LDNL HPD model and a 2.0-ms T_A Friedlander with matching PPLs.

REAT values for the Gunfender (open) are shown in blue and for the V-51R (simulated closed Gunfender) in red. Murphy's (2014 private communication between Dr William Murphy and Dr Joel Kalb; unreferenced) prediction appears acurate, since the V-51R REAT values approach those of the Gunfender as peak pressure of the stimulous waveform increases. The agreement is good at all frequencies. For the 190-dB pressure level, the model provides a conservative IL estimate; it underestimates the measured IL at most frequencies. The nonlinear model values chosen were R_{lk2} = 316, L_{lk2} = 0, K_{mat2} = 100, K_{cush2} = 0, and NL_{Power} = 1. The open single-orifice Gunfender is expected to be best described by Sivian's single orifice model, in which the resistance depends on the velocity raised to the first power (see Fig. 8).

The LDNL HPD model appropriately characterizes a hearing protector when the modeled ILs accurately match the progression of the measured ILs from low peak pressure waveforms to high peak pressure waveforms, for waveforms with the same specific time-dependence. Low peak pressure waveform ILs are approximately given by REAT IL measurements for the open earplug, while high peak pressure waveform ILs are approximately given by REAT ILs for the closed earplug.

However, as shown in Figs. 11–13, precise IL values for LDNL HPDs depend not only on the specific amplitude of the stimulus waveform but also on the specific time-dependence of the stimulus waveform.

6. Using a Single Waveform Source to Measure and Predict Insertion Losses

Ideally, frequency-dependent amplitudes with and without the hearing protector should be measured for the same impulsive waveform but this is not possible because it requires simultaneous measurements both with and without the hearing protector. Since ILs for LDNL HPDs depend on both the waveform's amplitude and time dependence, considerable inaccuracy can arrise in fitting ILs measured with waveforms from different sources that change in both the amplitude and the time dependence of the waveform. This was demonstrated in Figs. 11–14.

In attempts to minimize variations in IL due to waveform variations, we have used waveforms from a single source to measure and model ILs. We have used waveforms produced by an M4 rifle. Even when a single source is used, shot-to-shot variation can still produce inaccuracies, but using a single waveform source will more closely demonstrate how well a single LDNL HPD model charactrization can predict measured IL for a series of test waveforms.

Measurements of IL have been performed with the QRI-CAE selector dial HPD. These measurements were made with an ISL auditory test fixture (instrumented manikin head) exposed to M4 rifle muzzle blasts at various distances from the muzzle. The experiments are illustrated in Fig. 15.

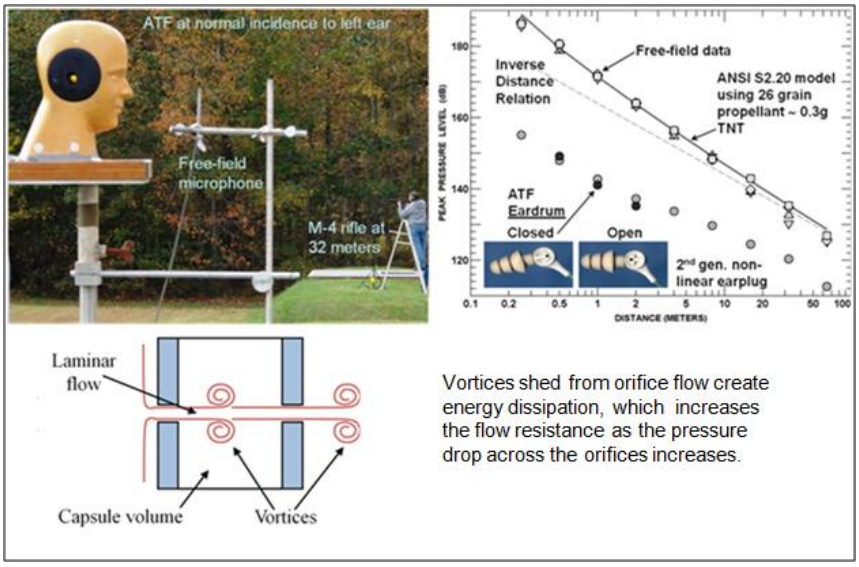

Fig. 15 An ISL auditory test fixture with hearing protection was exposed to M4 rifle muzzle blasts at various distances from the muzzle as shown in the upper left. Peak pressure levels of the free field muzzle blasts at the location of the auditory test fixture are shown in the upper right. A depiction of the vortex shedding that produces nonlinear resistance in the air flow through the dual orifice is shown in the lower left, and a description of the nonlinear resistance process is given in the lower right.

Figure 16 shows gray curves representing IL measurements under the QRI-CAE (selector dial) HPD at normal incidence on the ISL head as from top to bottom at distances of 64, 32, 16, 8, 4, 2, 1, 0.5, and 0.25 m perpendicular to the line of fire from an M4 rifle muzzle. The peak pressure levels for the gray curves from top to bottom were 126, 133, 139, 149, 155, 163, 172, 179, and 187 dB, respectively.

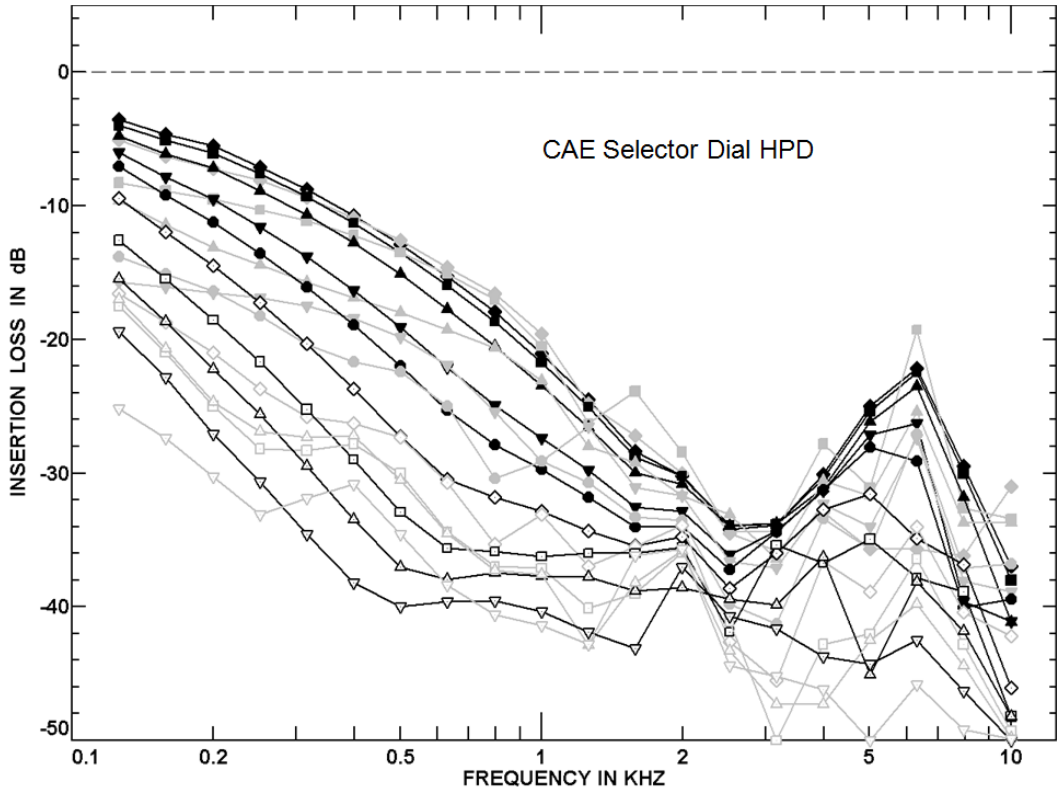

Fig. 16 QRI-CAE (selector dial) IL curves in gray measured in ATF for blasts with 110-190 dBP, nonlinear model using 0.3-ms duration Friedlander with matching PPL shown in black.

Lacking detailed REAT measurements for the QRI-CAE (selector dial) HPD, the closed IL level was chosen to be the lowest curve (highest IL) at 0.25 m and 187 dB, while the open IL level was chosen to be the highest curve (lowest IL) at 64 m and 126 dB. The agreement is good at frequencies above 0.2 kHz. The nonlinear model values chosen were $R_{lk2} = 316$, $L_{lk2} = 0$, $K_{mat2} = 100$, $K_{cu2} = 0$, and $NL_{Power} = 2$. (Units for each quantity are shown in Eq. 6.) The nonlinear double orifice plug in the QRI-CAE (selector dial) HPD is about two-thirds the size of the plug in the dual-ended CAE HPD. We believe this size difference and the physical differences between the QRI-CAE and the dual-ended CAE plug geometries are responsible for changing the nonlinear values for the QRI-CAE (selector dial) HPD with respect to the values for the dual-ended CAE HPD. Further, Fig. 16 shows that like the dual-ended CAE HPD, the QRI-CAE (selector dial) HPD also shows some resonance behavior at frequencies around 6.3 kHz. This resonance remains to be further studied, but the LDNL HPD model can be parameterized to display resonance behaviors similar to those observed in measurements.

7. Validation by Waveform Comparison

An accurate model of HPD performance should not only reproduce frequency and amplitude dependent IL, it should also determine the time-dependent waveform beneath the HPD. Though precise waveform reproduction may be desirable, sufficient accuracy will be achieved if the predicted waveforms accurately support assessments of hearing risk, for any validated method of hearing risk assessment. To further examine the application validity of the LDNL HPD model, we compare measured and predicted waveforms under a LDNL HPD.

By using the measured waveforms for the dual-ended CAE HPD, Figs. 17–21 show the grazing incidence measurements taken on the dual-ended CAE HPD in the ISL ATF at 0.25, 0.5, 1, 2, 4, 8, 16, 32, and 64 m from the muzzle of an M4 rifle. Free-field results are shown in blue while measurements are in red and predictions are in green. The top panel shows the energy spectrum of the waveforms, which are shown in the panel below. The middle panel shows the 3 waves plotted on the same scale and the bottom shows the waveforms predicted and measured under the HPD.

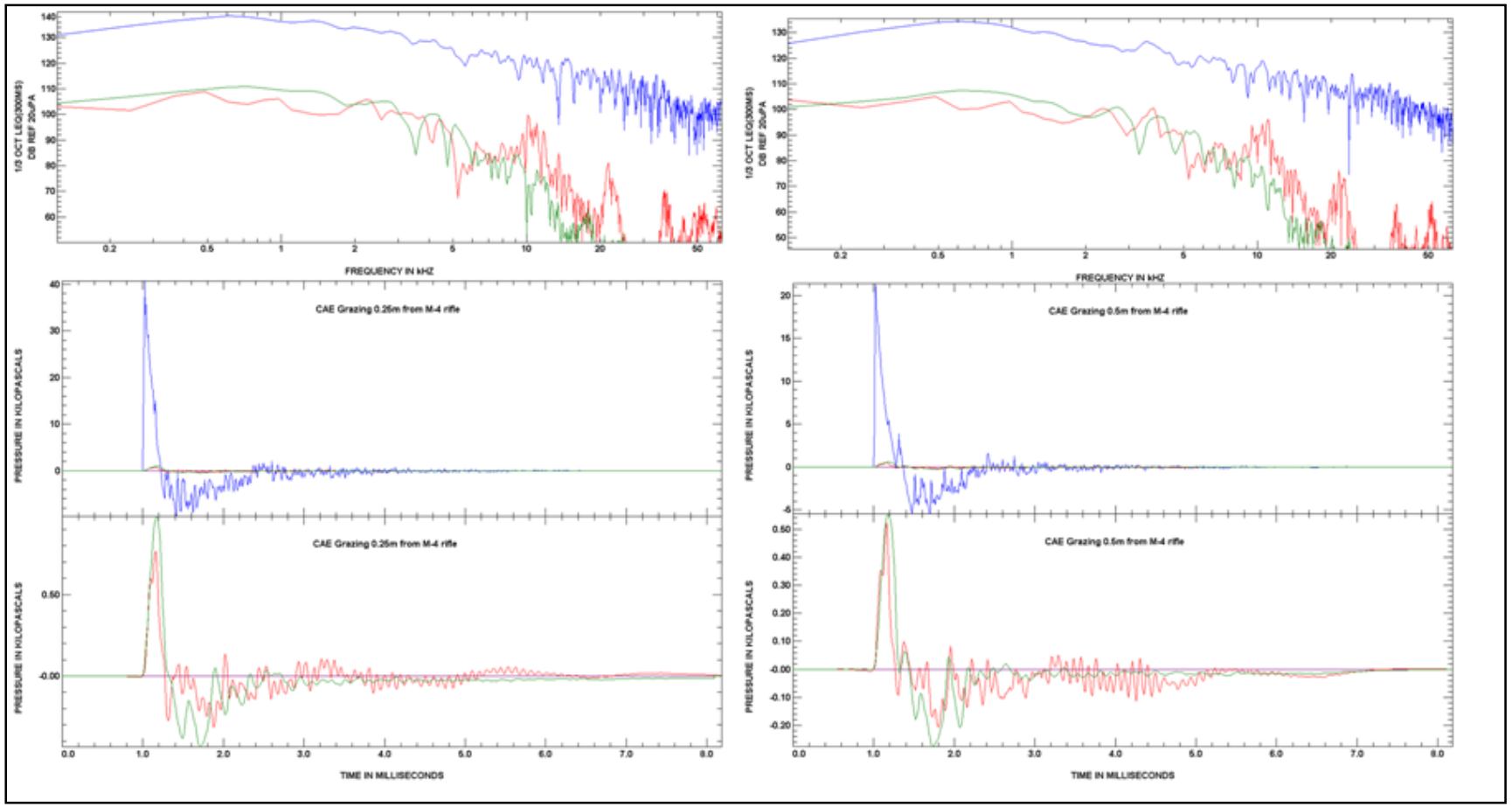

Fig. 17 Grazing incidence on open-mode CAE dual-ended HPD in ATF from M4 rifle muzzle perpendicular to line of fire at 0.25 m on left and 0.5 m on right. Waveforms in free-field are blue, under the protector measured in red, and predicted in green. Frequency spectra are shown on top, full-scale superimposed waveforms are shown in the middle, and expanded waves under the protector are on the bottom.

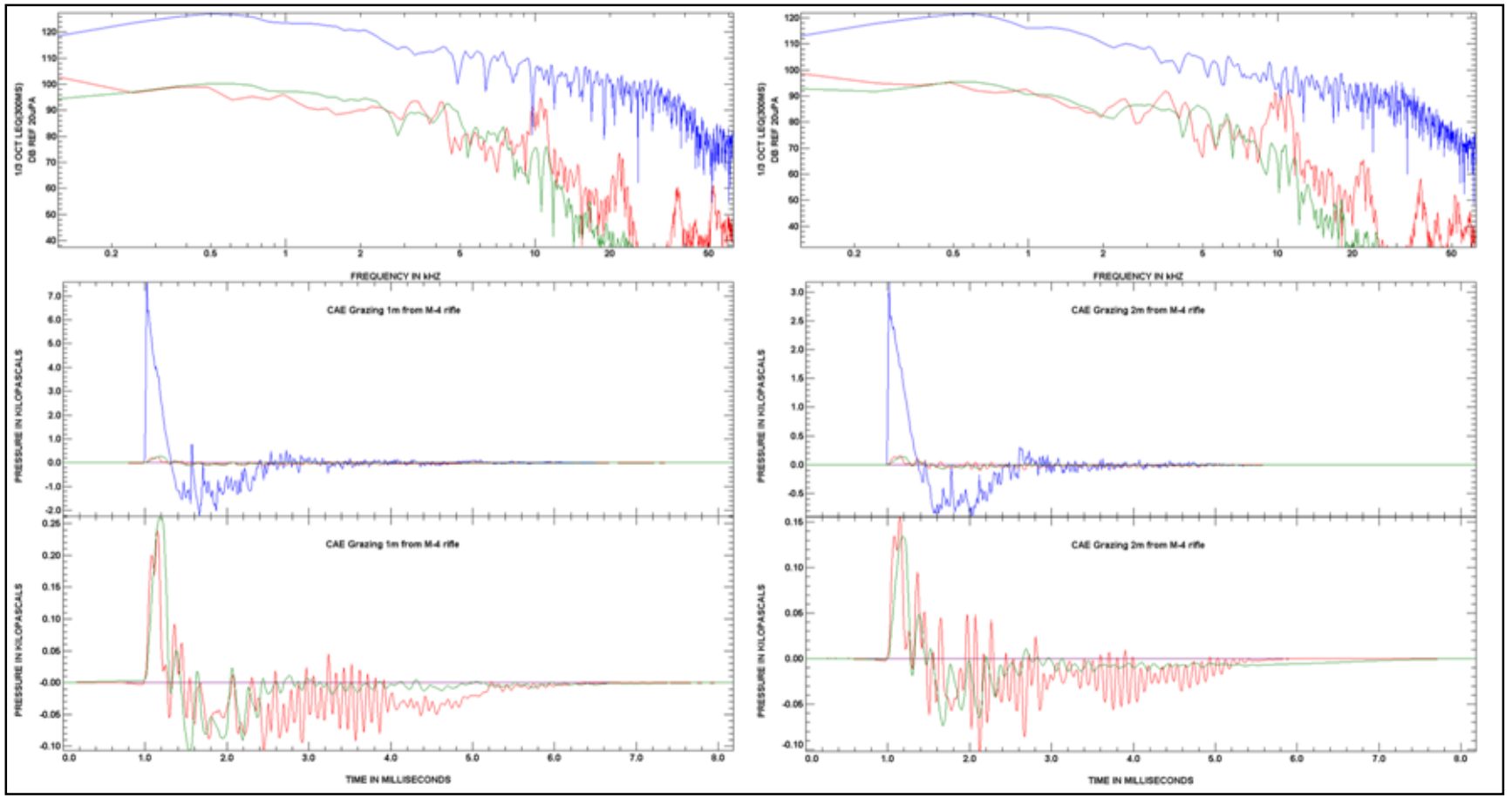

Fig. 18 Grazing incidence on open mode dual-ended CAE HPD in ATF from M4 rifle muzzle perpendicular to line of fire at 1 m on left and 2 m on right. Waveforms in free-field are blue, under the protector measured in red, and predicted in green. Frequency spectra are shown on top, full-scale superimposed waveforms are shown in the middle, and expanded waves under the protector are on the bottom.

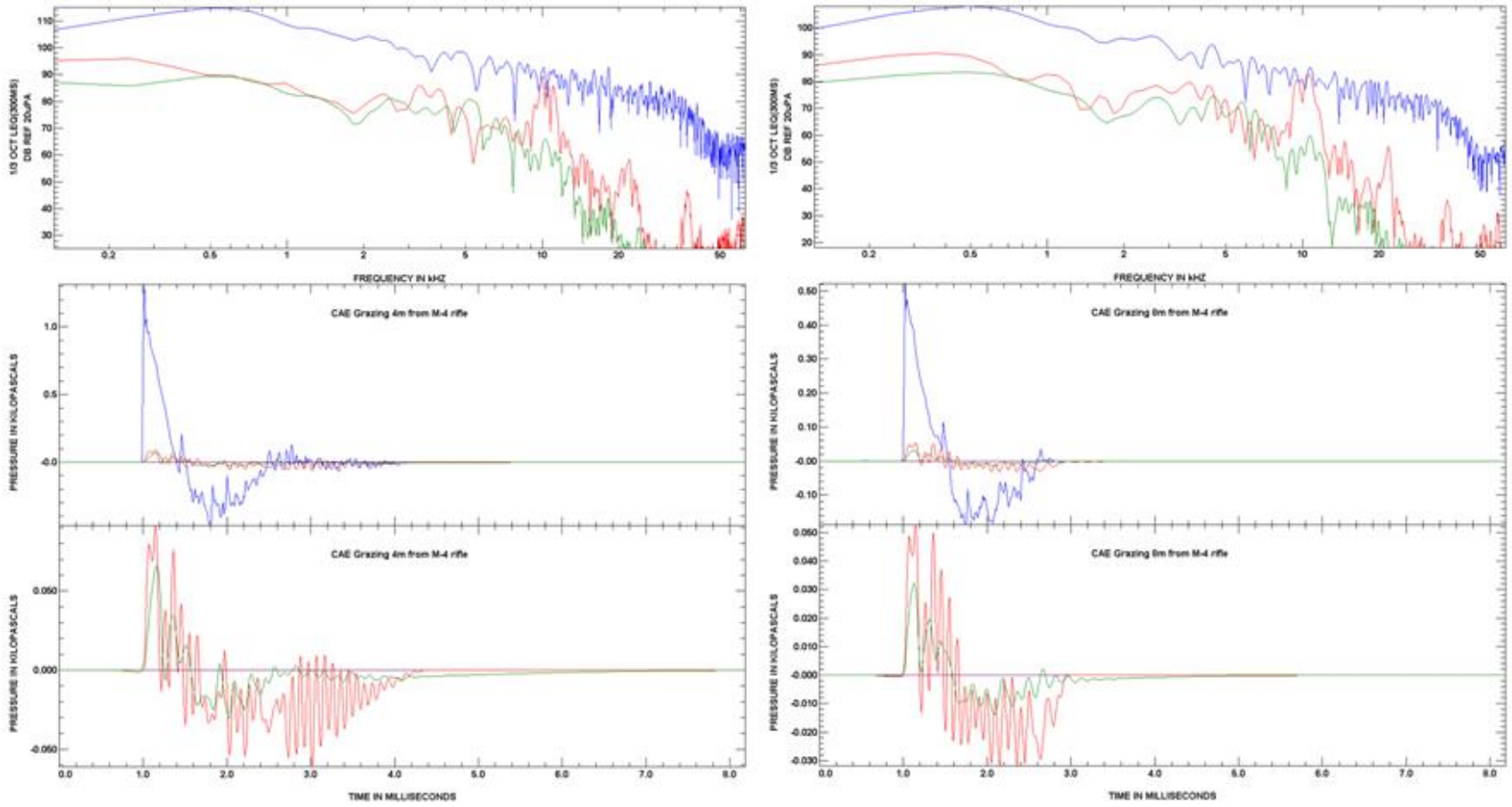

Fig. 19 Grazing incidence on open mode dual-ended CAE HPD in ATF from M4 rifle muzzle perpendicular to line of fire at 4 m on left and 8 m on right. Waveforms in free-field are blue, under the protector measured in red, and predicted in green. Frequency spectra are shown on top, full-scale superimposed waveforms are shown in the middle, and expanded waves under the protector are on the bottom.

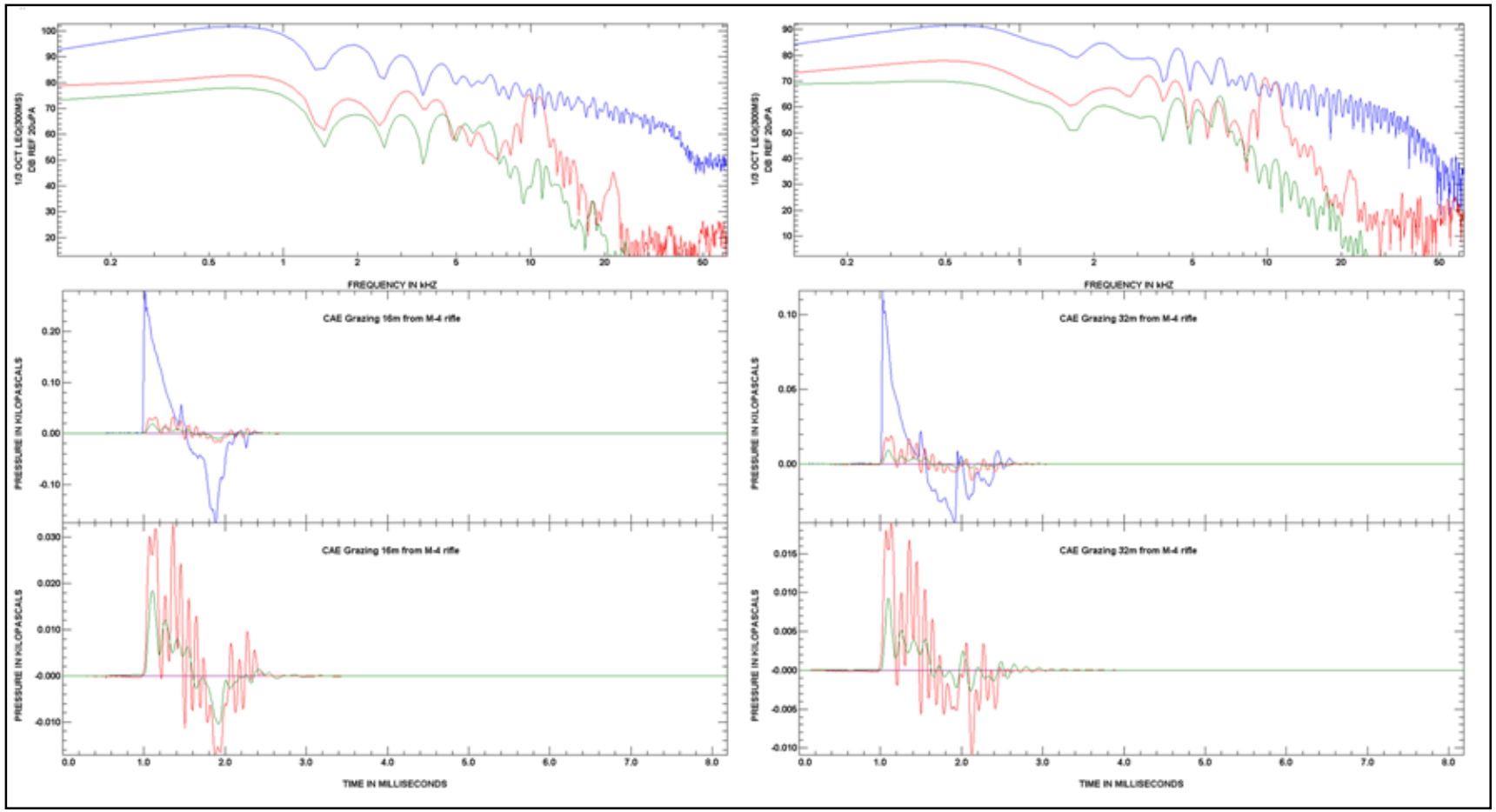

Fig. 20 Grazing incidence on open mode CAE dual-ended HPD in ATF from M4 rifle muzzle perpendicular to line of fire at 16 m on left and 32 m on right. Waveforms in free-field are blue, under the protector measured in red, and predicted in green. Frequency spectra are shown on top, full-scale superimposed waveforms are shown in the middle, and expanded waves under the protector are on the bottom.

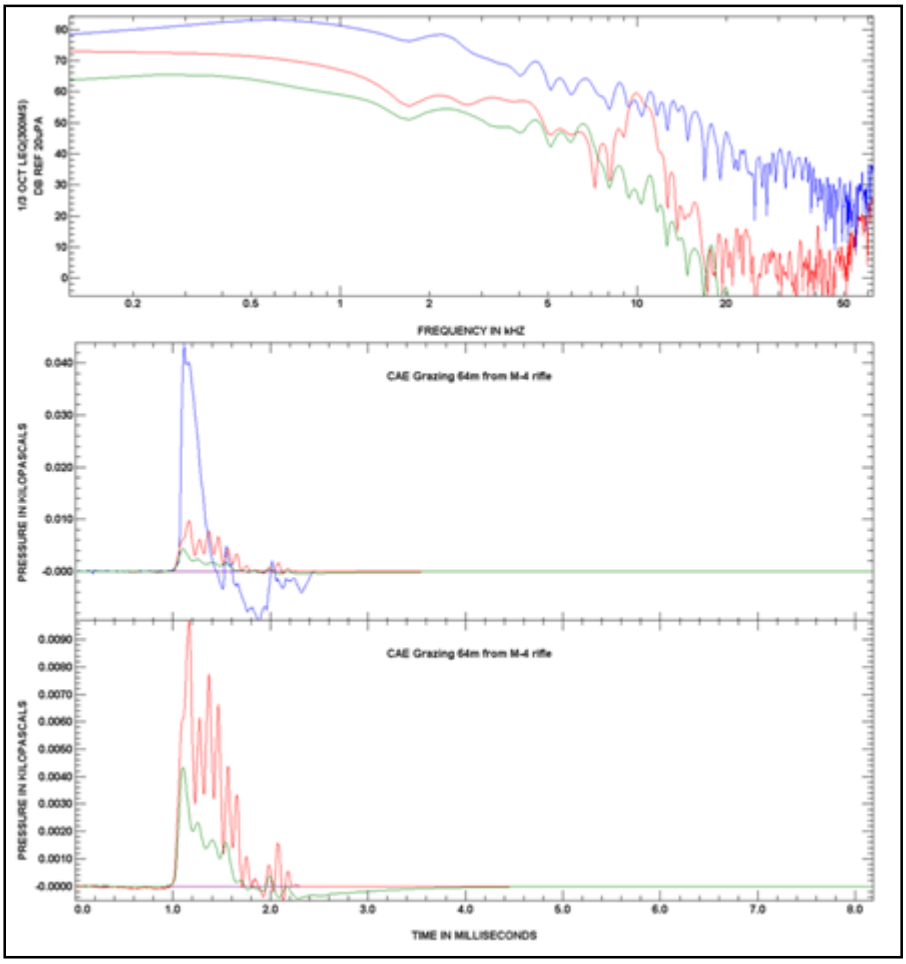

Fig. 21 Grazing incidence on open mode dual-ended CAE HPD in ATF from M4 rifle muzzle perpendicular to line of fire at 64 m. Waveforms in free-field are blue, under the protector measured in red, and predicted in green. Frequency spectra are shown on top, full-scale superimposed waveforms are shown in the middle, and expanded waves under the protector are on the bottom.

As noted earlier, waveform measurements under the dual-ended CAE HPD show an amplitude-dependent resonance near 6.3 kHz. This resonance is not strongly evident in REAT measurements at 4 and 8 kHz, which are used to fit model parameters for the dual-ended HPD. While less pronounced resonance in the dual-ended CAE HPD model can produce under-the-protector predicted pressures somewhat lower than measured pressures, the differences are small, especially when compared with the amplitude of the original free-field waveform.

This HPD resonance may be due to vibrations in the part of the dual-ended CAE that extends outside the ear. The external part of the dual-ended CAE is greater than the external portions of most other earplugs such as the QRI-CAE (selector dial) HPD and the Gunfender. Alternately, it may be due to a resonance between the orifices in the HPD. We have yet to determine a specific cause for the resonance.

Even though the resonance is present, the peaks of the predicted pressures decrease consistently with the peaks of the measured pressures as the distance increases and the stimulus waveform pressures fall and the HPD approaches linear behavior.

Figures 22–26 show the measurements taken using normal incidence QRI-CAE (selector dial) HPD in the ISL ATF at 0.25, 0.5, 1, 2, 4, 8, 16, 32, and 64 m from the M4 rifle muzzle. Again, the free-field results are shown in blue while measurements are in red and predictions are in green. The top panel shows the energy spectrum of the waveforms, which are shown in the panel below. The resonance in the CAE measurements seen at 10 kHz does not appear in the QRI, possibly because there is less exposed structure outside the ear. The energy spectrums for the measured and predicted waves under the protector agree at frequencies up to the maximum modeled frequency of 8 kHz. The stimulus waveforms decrease in amplitude with distance from the muzzle. As the more distant, lower amplitude stimuli interact with the HPD, the nonlinearity is reduced.

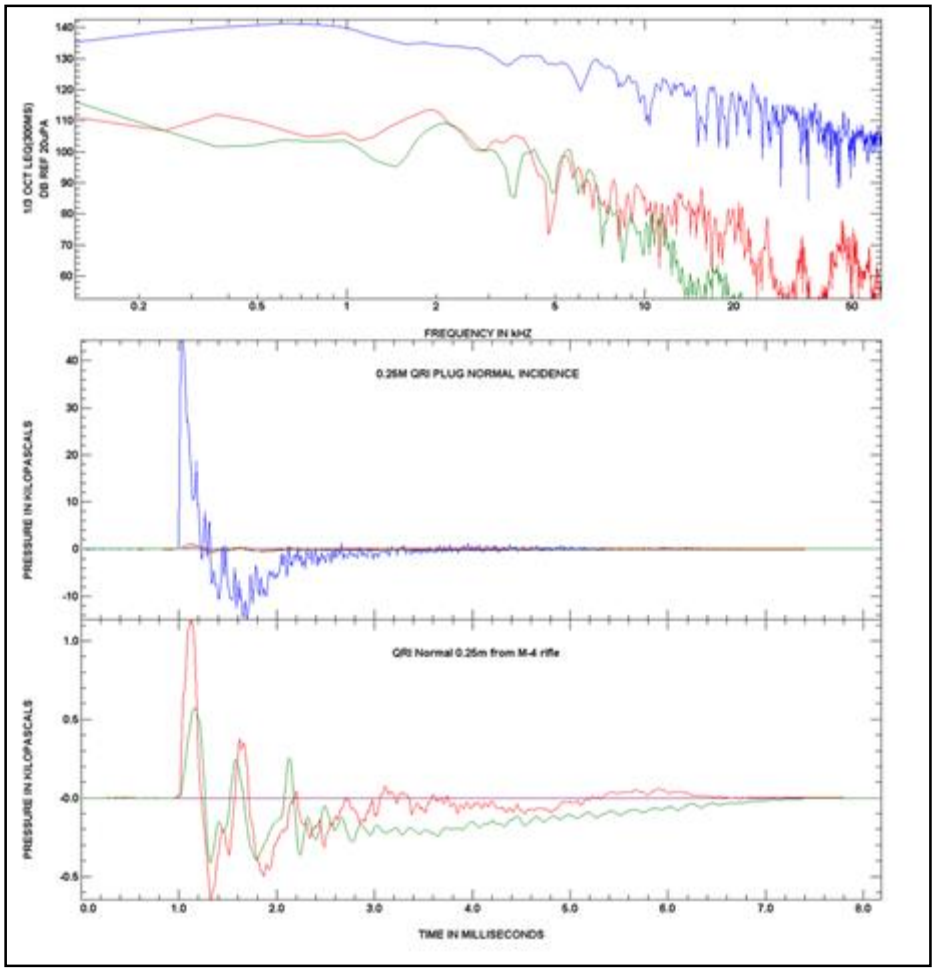

Fig. 22 Normal incidence 0.25 m from the open mode QRI-CAE (selector dial) HPD. Waveforms in free-field are blue, under the protector measured in red, and predicted in green. Frequency spectra are shown on top, full-scale superimposed waveforms are shown in the middle, and expanded waves under the protector are on the bottom.

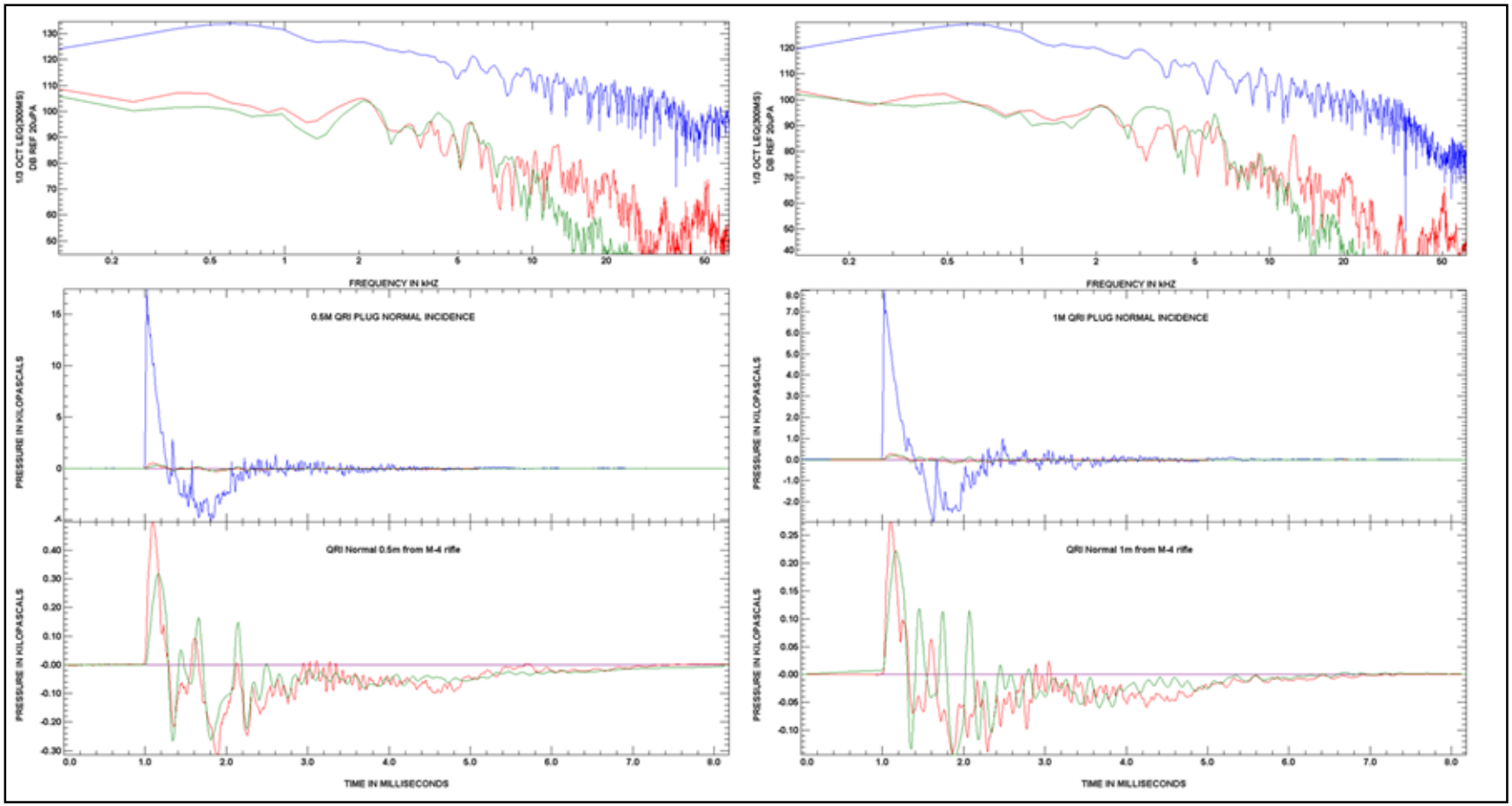

Fig. 23 Normal incidence on open mode CAE selector dial HPD in ATF from M4 rifle muzzle perpendicular to line of fire at 0.5 m on left and 1 m on right. Waveforms in free-field are blue, under the protector measured in red, and predicted in green. Frequency spectra are shown on top, full-scale superimposed waveforms are shown in the middle, and expanded waves under the protector are on the bottom.

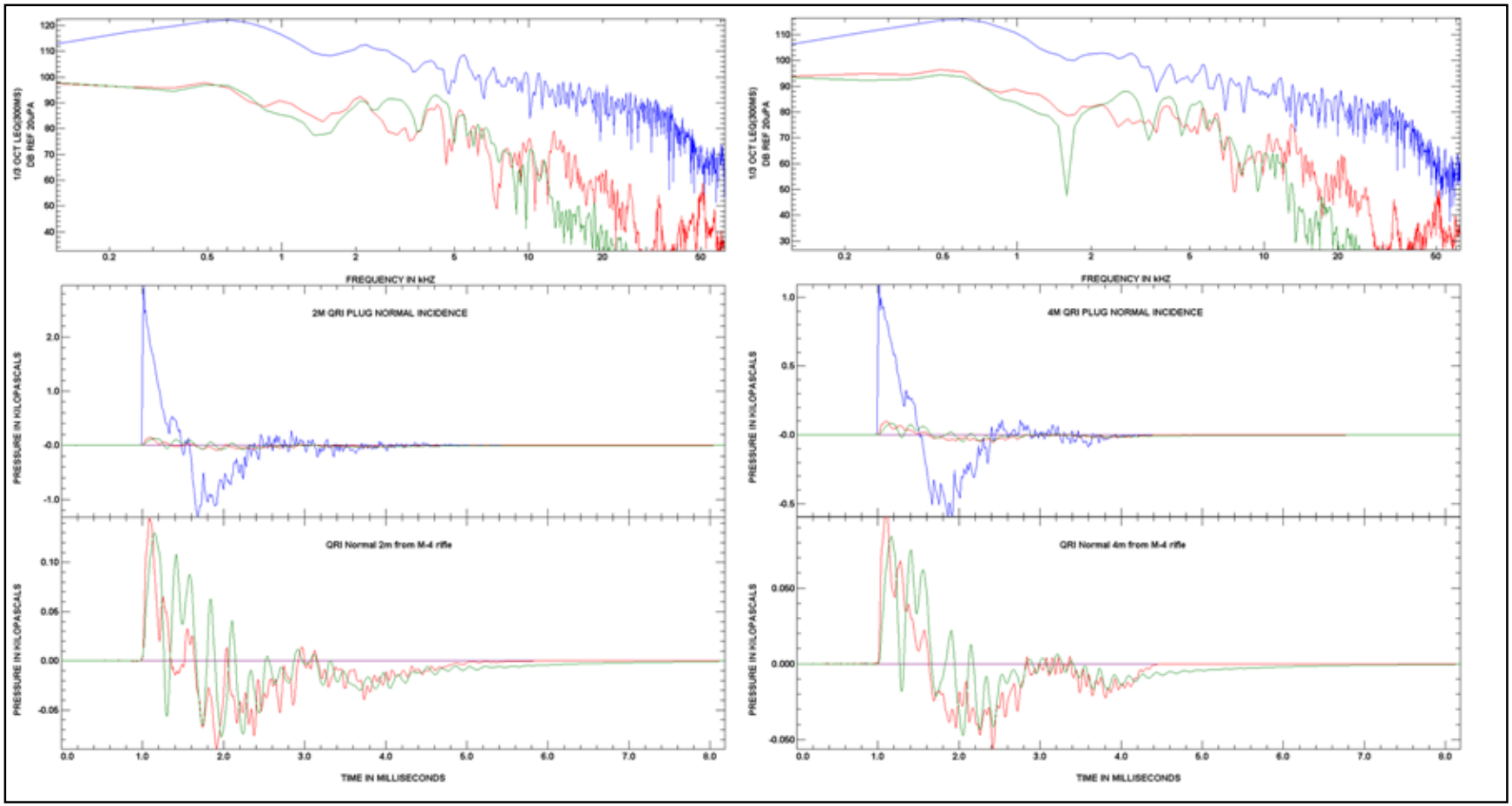

Fig. 24 Normal incidence on open mode CAE selector dial HPD in ATF from M4 rifle muzzle perpendicular to line of fire at 2 m on left and 4 m on right. Waveforms in free-field are blue, under the protector measured in red, and predicted in green. Frequency spectra are shown on top, full-scale superimposed waveforms are shown in the middle, and expanded waves under the protector are on the bottom.

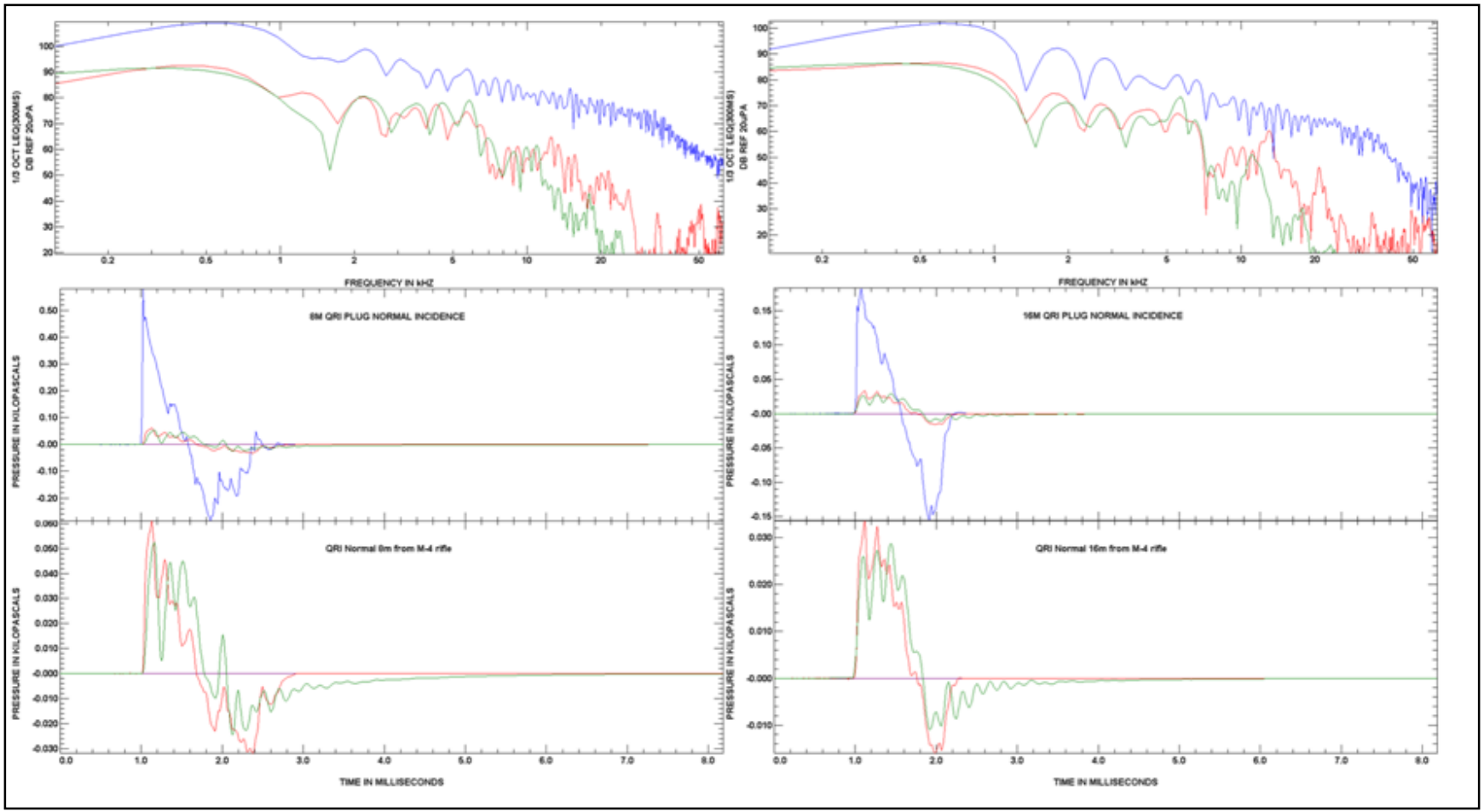

Fig. 25 Normal incidence on open mode CAE selector dial HPD in ATF from M4 rifle muzzle perpendicular to line of fire at 8 m on left and 16 m on right. Waveforms in free-field are blue, under the protector measured in red, and predicted in green. Frequency spectra are shown on top, full scale superimposed waveforms are shown in the middle, and expanded waves under the protector are on the bottom.

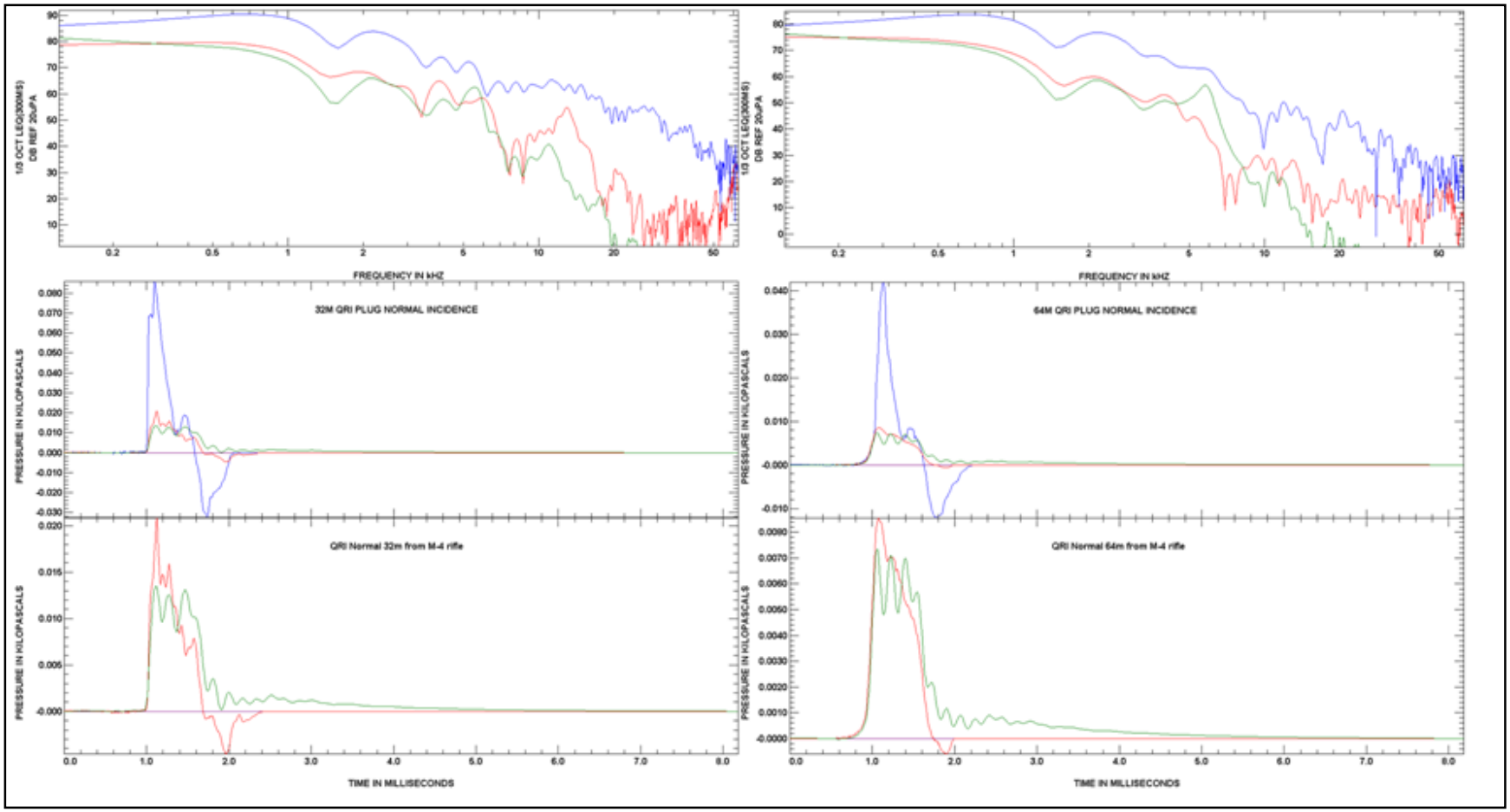

Fig. 26 Normal incidence on open mode CAE selector dial HPD in ATF from M4 rifle muzzle perpendicular to line of fire at 32 m on left and 64 m on right. Waveforms in free-field are blue, under the protector measured in red, and predicted in green. Frequency spectra are shown on top, full-scale superimposed waveforms are shown in the middle, and expanded waves under the protector are on the bottom.

The predicted and measured waveforms show good agreement to within 3 dB. The CAE selector dial HPD in the ATF shows no ringing at frequencies above 10 kHz, as seen in the dual-ended CAE HPD. Peak pressures and general waveform time-dependence remain in close agreement over the range of distances that correspond to varying peak pressures for these impulsive waveform stimuli.

8. Application of the Measured and Predicted Waveforms in Hearing Risk Assessment

Exactly matching predicted waveforms with waveforms measured in tests is a conclusive demonstration of model validity. However, as was seen in the IL calculations, the IL for a LDNL HPD changes with both the amplitude and the time-dependence of the stimulus waveform. Thus, the ability to accurately predict waveforms beneath HPDs cannot be guaranteed for all stimulus waveforms by fitting the IL characteristics for a particular specific stimulus waveform or even a finite specific set of waveforms. However, the ability of the LDNL HPD model to accurately predict IL for waveforms over a limited range of amplitude and time dependence variations can provide valid risk assessments for some range of varied stimulus waveforms.

The purpose of calculating or predicting the waveform beneath the HPD is to assess the potential risk to hearing for a person wearing the HPD. Once it is established that ATFs provide valid representations of humans, we believe ATFs offer the best method of testing HPD performance without risking damage to the hearing of test participants. However, it would be impractical to perform test measurements with all waveforms at all distances with all hearing protectors. Thus, predictive model capability for the purpose of hearing protection evaluation remains essential. To provide validation for the purpose of evaluating hearing risk, we have calculated various hearing risk characterization parameters, such as the allowed number of rounds (ANOR), the auditory risk units (ARUs), and the A-weighted energy, and we compare these characteristics as they are determined for measured and for predicted waveforms.

The A-weighted energy of a waveform is often used as a meaningful characteristic of a waveform. Although many different time and amplitude dependencies of waveforms can result in the same A-weighted energy, energy is a well-defined physical quantity and provides some insight regarding the waveform.

Figure 27 shows the A-weighted energy in the waveforms measured and predicted under the CAE selector dial HPD used in the ISL ATF, as a function of distance from the rifle muzzle.

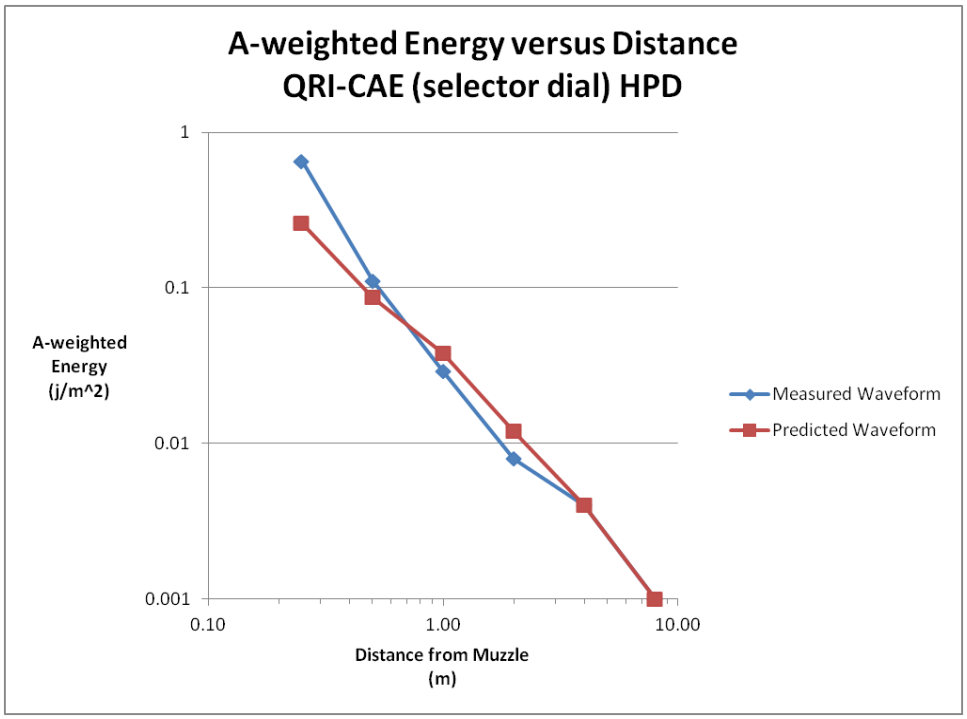

Fig. 27 A-weighted energy under the QRI-CAE (selector dial) HPD measured and predicted as a function of distance from the rifle muzzle for normal incidence

Figure 27 shows (once the error in the 0.5 m measurement calculation is addressed) that the waveforms predicted by the LDNL HPD model appropriately reflect the A-weighted energy of the waveform measured under the HPD.

Figure 28 shows the A-weighted energy in the waveforms measured and predicted under the dual-ended CAE HPD used in the ISL ATF, as a function of distance from the rifle muzzle.

Figure 28 shows that the waveforms predicted by the LDNL HPD model appropriately reflect the A-weighted energy of the waveform measured under the dual-ended CAE HPD.

Figure 28 shows a consistently changing discrepancy between the A-weighted energies derived from measured and predicted waveforms under the HPD. As described earlier, the dual-ended CAE exhibits an amplitude-dependent resonant behavior in frequencies near 6.3 kHz. This frequency range is not well captured by REAT measurements and resonance in this frequency range often is not apparent in REAT measurements. When REAT measurements are used as a basis in the LDNL HPD model, the model will not reflect this resonance behavior. This resonance in the measured waveforms results in an amplitude dependent difference between the hearing risks associated with the measured and predicted waveforms, as Fig. 28 shows.

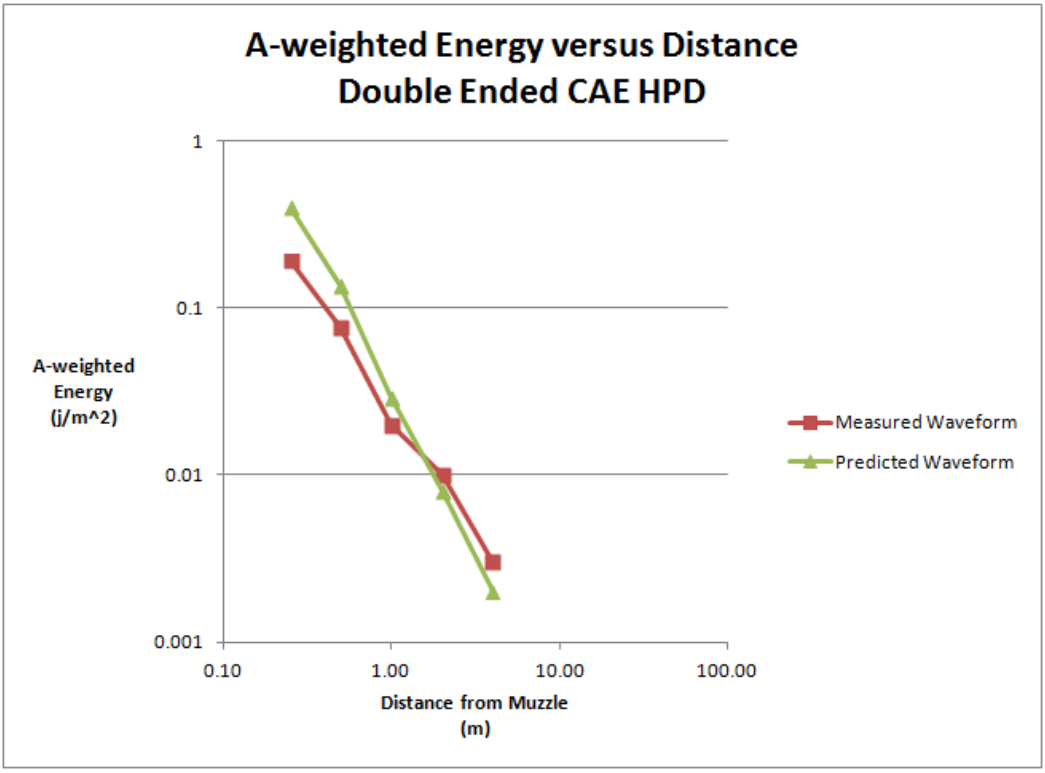

Fig. 28 A-weighted energy under the dual-ended CAE HPD measured and predicted as a function of distance from the rifle muzzle for the normal incidence

The ANOR is an important parameter in assessing the effectiveness of an HPD in providing protection against weapon fire. AHAAH calculates the ANOR value from the auditory risk units determined for the waveform. The ARU has a direct relation to the physical damage caused by exposure to the impulsive waveform stimulus; ARUs are physically related to the displacements, strains, and damages calculated along the basilar membrane in the cochlea. A total of 500 ARUs is the maximum allowable "dose" for occasional exposures within a 24-h period. Doses greater than 500 ARUs are predicted to produce significant probability of permanent hearing loss. For daily or near daily exposures, the lower limit of 200 ARUs is advisable to limit damage accumulation. Using 500 ARUs as the total allowed limit in a 24-h period, we determine the number of identical impulsive stimuli that will result in a total of 500 ARUs. When dealing with weapons fire, that number of allowed exposures is the ANOR.

We compare the ANOR calculated from the measured waveform under the HPD to the ANOR calculated from the predicted waveform under the HPD.

Figure 29 shows the measured and the predicted waveform ANORs for the QRI-CAE (selector dial) HPD for the warned AHAAH condition at different distances from the rifle muzzle.

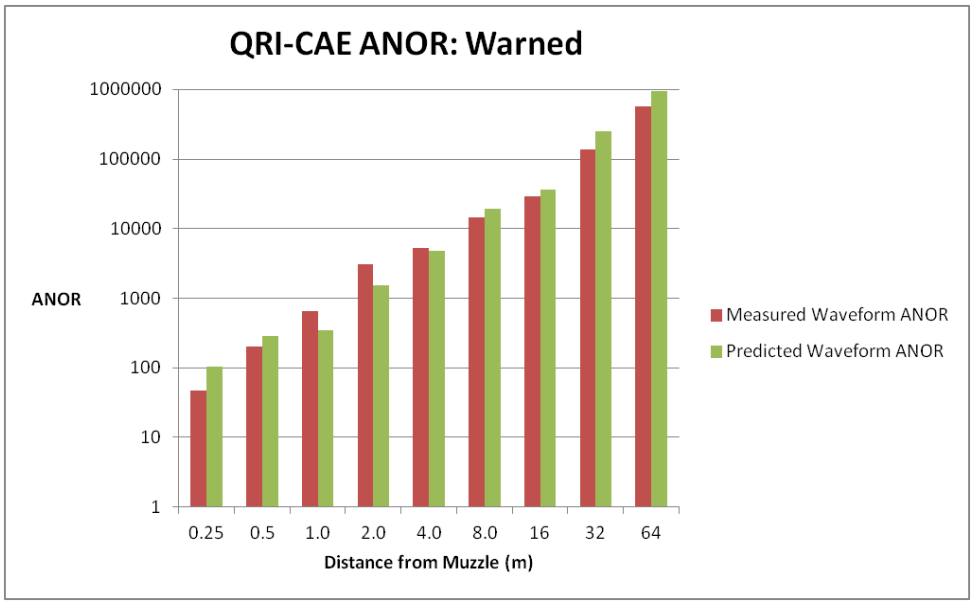

Fig. 29 The measured and predicted ANORs for the QRI-CAE (selector dial) HPD in the warned AHAAH condition

Figure 29 shows the LDNL HPD model consistently provides predicted waveforms that accurately determine the ANOR for the QRI-CAE (selector dial) HPD in the warned AHAAH condition.

Similarly, Fig. 30 shows the measured and the predicted waveform ANORs for the dual-ended CAE HPD for the warned AHAAH condition at different distances from the rifle muzzle.

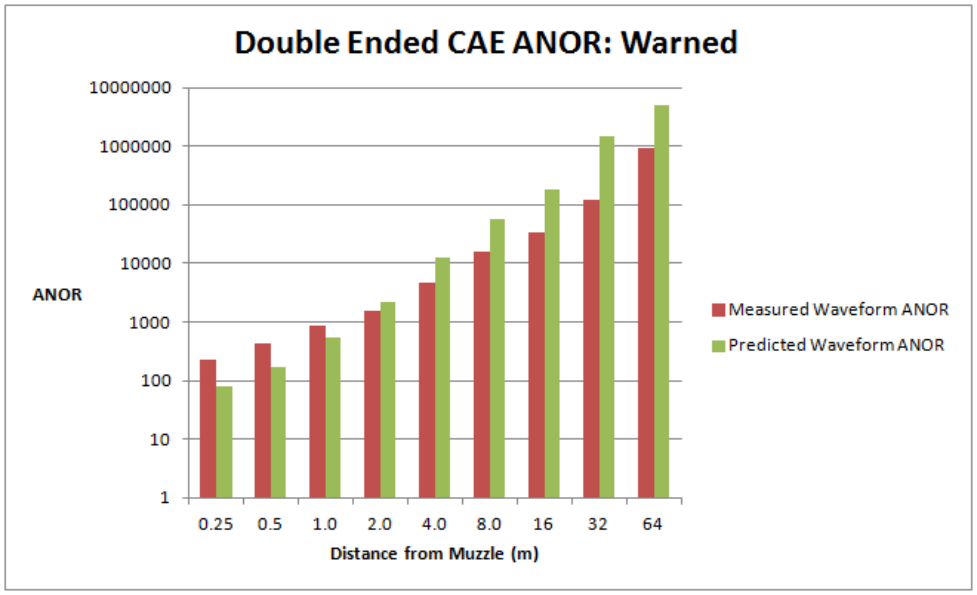

Fig. 30 The measured and predicted ANORs for the dual-ended CAE HPD in the warned AHAAH condition

Again, the dual-ended CAE exhibits an amplitude-dependent resonant behavior that results in an amplitude dependent difference between the hearing risks associated with the measured and predicted waveforms. The model remains conservative at close distances where hazards are greatest, while the resonance causes an overestimate of the ANOR above 1,000 rounds. More detailed IL measurements for the dual-ended CAE will provide a more accurate characterization of the HP in the model.

The AHAAH also applies an unwarned condition. We expect an exposed individual would begin to anticipate continued exposures after a series of exposures. However, as a characteristic for evaluating the risk of hearing damage, we still can apply an unwarned condition and determine the number of exposures possible before incurring a significant risk of sustaining hearing damage for a fraction of exposed people. Figure 31 shows the measured and predicted waveform ANORs for the QRI-CAE (selector dial) HPD for the unwarned AHAAH condition, at different distances from the rifle muzzle.

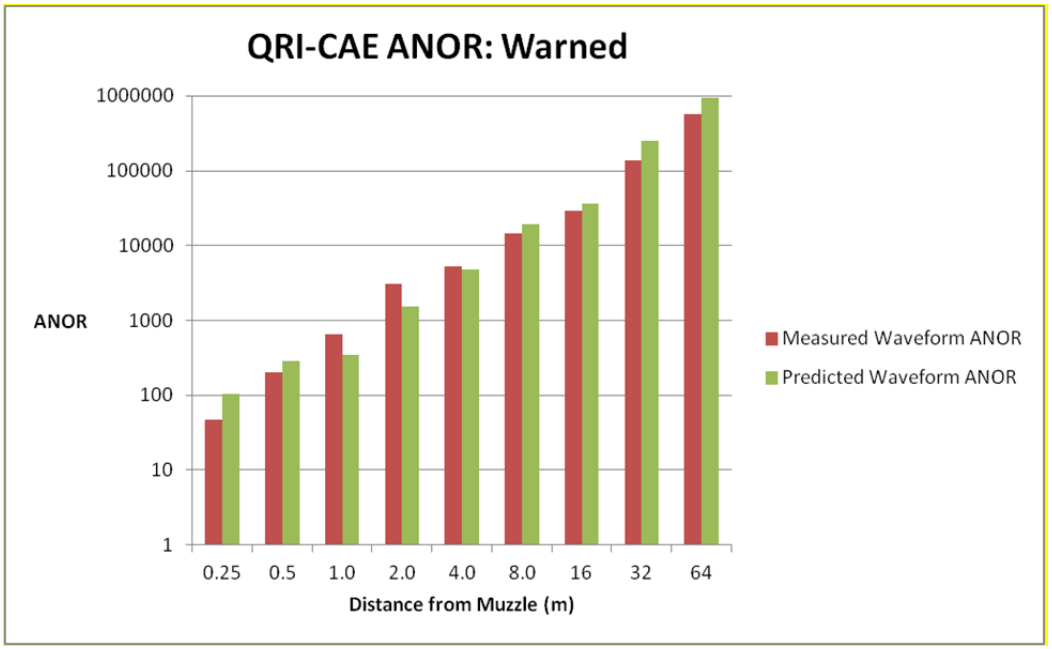

Fig. 31 The measured and predicted waveform ANORs for the QRI-CAE (selector dial) HPD in the unwarned AHAAH condition

Figure 31 shows the LDNL HPD model consistently provides predicted waveforms that accurately determine the ANOR for the CAE selector dial HPD in the unwarned AHAAH condition. The unwarned condition is significantly more hazardous than the warned condition. Although we still can apply an unwarned condition and determine the number of exposures possible before incurring a significant increase in the risk of sustaining hearing damage for a fraction of

exposed people, in practical situations, after a significant number of exposures, we would anticipate an exposed individual would most likely begin to anticipate the continued exposures.

Figure 32 shows the measured and predicted waveform ANORs for the dual-ended CAE HPD for the unwarned AHAAH condition, at different distances from the rifle muzzle.

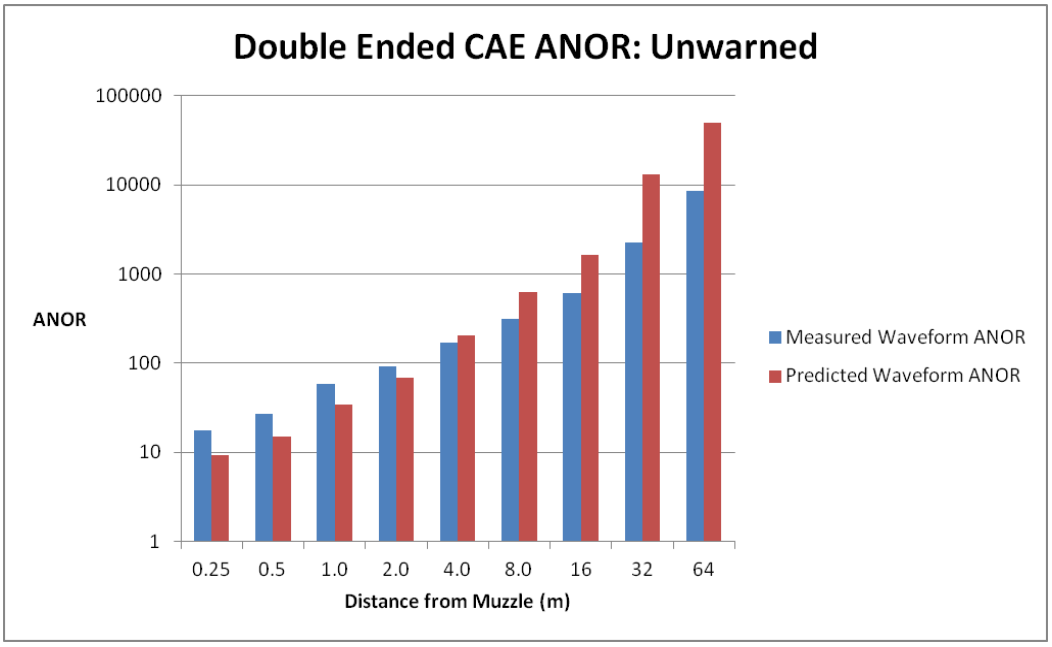

Fig. 32 The measured and predicted waveform ANORs for the dual-ended CAE HPD in the unwarned AHAAH condition

Figure 32 shows ANOR values calculated from waveforms predicted by the LDNL HPD model show some amplitude-dependent deviations from ANOR values calculated from waveforms measured under the dual-ended CAE. As previously described, we believe this deviation is largely due to an insufficient characterization of the resonance observed in waveforms measured under the dual-ended CAE in the ATF.

As mentioned earlier, AHAAH calculates and expresses risk of hearing damage in terms of ARUs. Predicted and measured HPD performance is illustrated in terms of ARUs in Figs. 33 and 34.

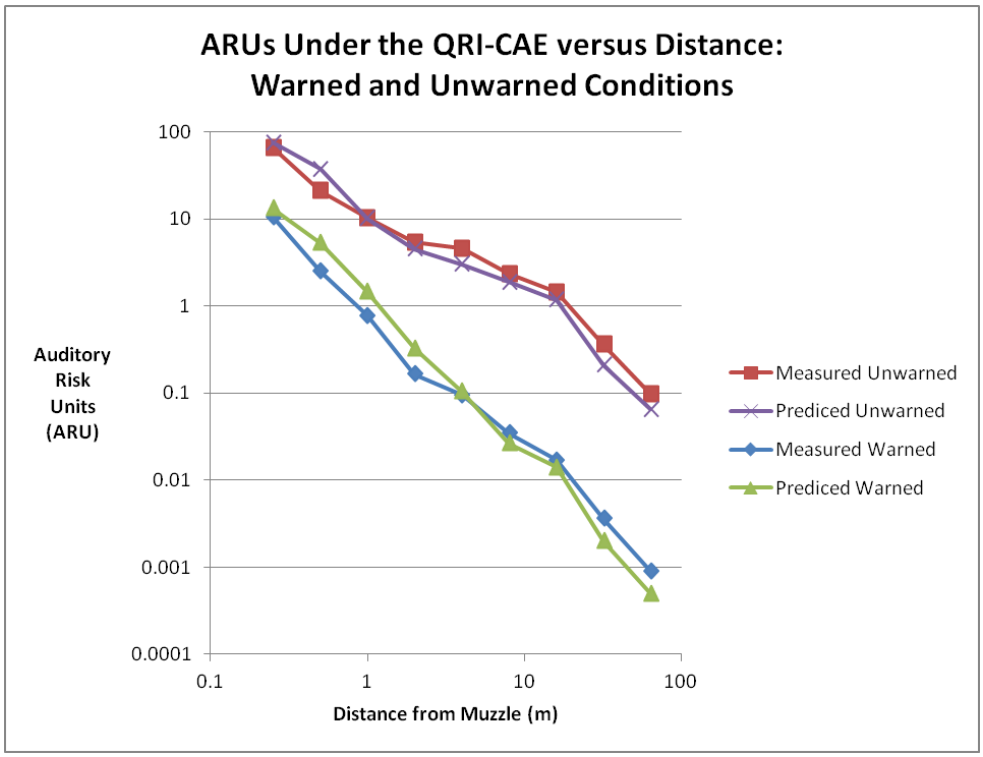

Fig. 33 ARU values for measured and predicted waveforms under the QRI-CAE (selector dial) HPD for unwarned and warned conditions

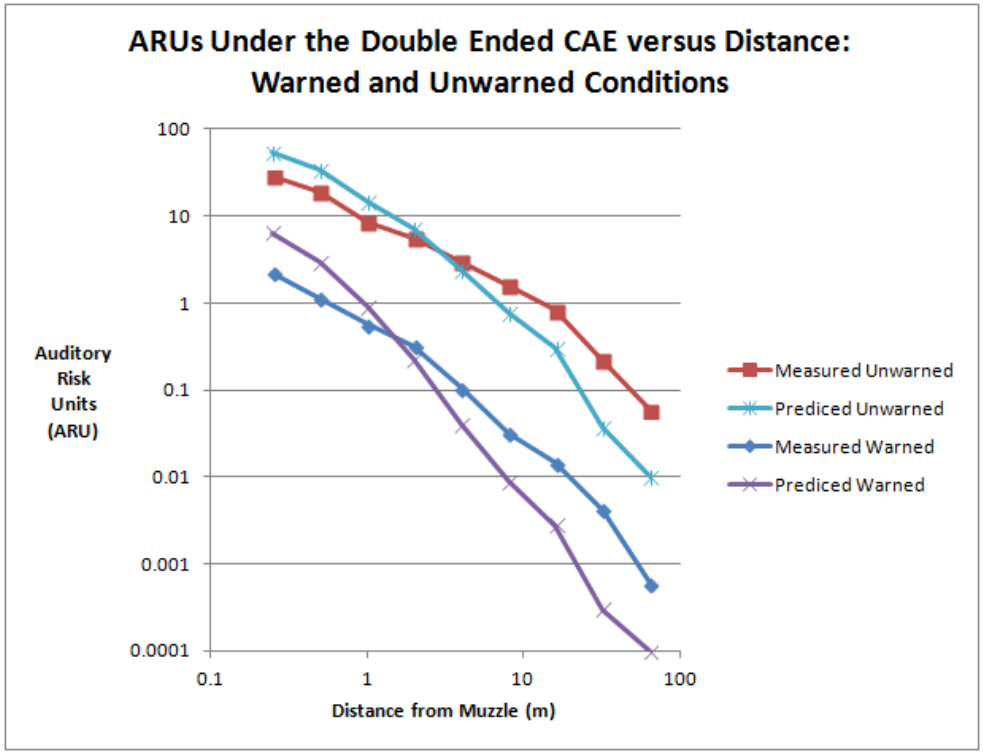

Fig. 34 The measured and predicted ARU values for the CAE dual-ended HPD in the warned AHAAH condition

Figure 33 shows the ARU values for measured and the predicted waveforms beneath the QRI-CAE (selector dial) HPD as functions of distance from the rifle muzzle. Both warned and unwarned ARU values are compared.

Figure 33 shows the LDNL HPD model consistently provides predicted waveforms that accurately determine the ARU value for the QRI-CAE (selector dial) HPD in the unwarned and warned condition.

Similarly, Fig. 34 shows ARU values for measured and the predicted waveforms beneath the dual-ended CAE HPD as functions of distance from the rifle muzzle. Both warned and unwarned ARU values are compared.

Figure 34 shows an increased discrepancy between the ARU values derived from measured and predicted waveforms under the HPD. As discussed earlier, the measured waveforms show an amplitude-dependent resonant behavior in the CAE dual-ended HPD in the 6.3-kHz frequency range. This frequency range is not well captured in REAT IL measurements used to characterize the hearing protector. Thus, the predicted waveforms do not include the full resonance effect included in the measured waveforms.

Overall, the comparisons of ARU values for these 2 HPDs show that the LDNL HPD model predicts waveforms that provide hearing risk evaluation characteristics that are consistent with the same characteristics determined from waveforms measured under the HPDs. The fact that the resonance in the high-frequency behavior of the CAE dual-ended HPD produced observable differences between the characteristics of the measured and predicated waveforms for this HPD emphasizes the need to accurately characterize the performance of the hearing protector over a sufficient range of frequencies. When this is done, as for the CAE selector dial HPD, the characteristics derived from measured and predicted waveforms show no practical differences.

9. Conclusions

Using IL data measured with test impulses of various amplitudes and time-dependencies, we have modeled the performance of LDNL hearing protectors using nonlinear characteristics of flow through orifices. Using electro-acoustic analysis, nonlinear electro-acoustic component expressions were adapted from the literature of nonlinear fluid dynamics in Sivian's (1935) measurements of flow through small orifices. We noted similar work done by Ingard (1967) but elected to apply Sivian's observations for determining nonlinear characteristic expressions.

To determine values describing specific level-dependent, nonlinear HPDs, we applied IL measurements performed with impulsive stimulus waveforms with

different peak pressure amplitudes. These IL measurements were performed by Berger and Hamery (2008) for the dual-ended CAE HPD and the Gunfender HPD. To perform these measurements, the hearing protector device is used in the ear of an auditory test fixture and a microphone is used under the hearing protector to measure the waveform beneath the protector. We also measured ILs with varied amplitude stimulus waveforms using the QRI CAE (with a selector dial) HPD. These measurements were made with an M14 rifle as the source of the impulsive waveform stimuli. Various distances between the muzzle and the auditory test fixture were used to obtain stimulus waveforms of varying amplitudes.

When the nonlinear parameters based on these measurements are used, the resulting nonlinear HPD model can be validated by comparing characteristics of the waveform predicted beneath the HPD to the same characteristics determined from the waveform measured beneath the HPD. Compared characteristics include the A-weighted energy, the ANOR, and the ARUs. Calculations with measured waveforms show agreement to within 3 dB, for both normal and grazing incidence. Calculated waveforms beneath 2 nonlinear earplugs determined from measured free-field waveforms at grazing and normal incidence show agreement with waveforms measured beneath the earplugs to within 3 dB across all waveform stimulus amplitudes, which included muzzle blast waveforms with peak pressures ranging from 124- to 187-dB peak pressure level. When the characterization of the dual-ended CAE HPD model failed to account for the 6.3-kHz resonance because IL is not well captured in REAT measurements and REAT measurements may not reflect this resonance, departures were observed between values derived from measured and predicted waveforms. We conclude that this departure illustrates that the LDNL HPD model is sensitive to hearing protector characterization, and if the hearing protector is better characterized, improved agreement between measured and predicted characteristics will be obtained, as was the case for the CAE selector dial HPD.

Overall, we conclude the LDNL HPD model is useful for predicting under-the-protector waveforms and subsequently using the predictions for accurately estimating the risk of hearing damage from exposure to impulsive waveform stimuli while using characterized HPDs.

10. Further Efforts

To support the application of this LDNL HPD model, we will be following up this report with a full description of the software process for fitting LDNL HPDs. This software will be made available with the AHAAH software.

We also will be creating a detailed description of the physical expressions and parameters used in the LDNL HPD model and the AHAAH, itself. This will illustrate the physical basis of the linear and nonlinear electro-acoustic components and parameters in the model and in the AHAAH, demonstrating that the hearing protector model and the AHAAH represent more than empirical representations of observed auditory data; rather they represent a dynamic, physically based, description of the actual mechanics of HPD and human ear performance. As such, these models have a greater probability of maintaining accuracy in extrapolated applications than do purely empirical models based only on empirical fits to observed data without any physical bases.

As an increasing number of LDNL HPDs become widely available, measurements to characterize these devices will be increasingly needed. Auditory test fixture measurements using stimulus waveforms covering a range of pressure amplitudes and time-dependencies will be essential in characterizing these LDNL HPDs and in establishing and verifying the ranges of applicability of these characterizations.

Although testing with auditory test fixtures is essential, we believe it is impractical to test every HPD against every possible waveform. Since IL is a function of the specific stimulus waveform amplitude and time-dependence, we believe the only practical method of assessing the protective performance of a LDNL HPD is to accurately characterize the device's nonlinear flow processes and apply that characterization in a modeled determination of IL for particular stimulus waveforms. We will extend efforts to standardize and validate auditory test fixtures and auditory test fixture testing for the characterization of LDNL HPDs.

11. References

Abramowitz M, Stegun IA. Handbook of mathematical functions. US Government Printing Office. Washington (DC): 1964; p. 897.

Bekesy GV. Paradoxical direction of wave travel along the cochlear partition. J. Acoust. Soc. Am. 1955;27.

Békésy GV. Experiments in hearing (Vol. 8). Wever EG, editor. New York (NY): McGraw-Hill; 1960.

Berger EH. Methods of measuring the attenuation of hearing protection devices. The Journal of the Acoustical Society of America. 1986;79(6):1655–1687.

Berger EH. Preferred methods for measuring hearing protector attenuation. In: Proceedings of Inter-Noise. 2005;5:58.

Berger EH, Hamery P. Empirical evaluation using impulse noise of the level-dependency of various passive earplug designs, acoustics '08 Paris. J. Acoustic Society of America. 2008;123(5-2):3528.

Buck K. Performance of different types of hearing protectors undergoing high-level impulse noise. International Journal of Occupational Safety and Ergonomics (JOSE). 2009;15(2):227–240.

Dancer A, Buck K, Hamery P, Zimpfer-Jost V. Protection and communication in extreme environments. Proc. ICBEN. 2003. p. 5–10.

Dancer A, Grateau P, Cabanis A, Barnabé G, Cagnin G, Vaillant T, Lafont D. Effectiveness of earplugs in high-intensity impulse noise. The Journal of the Acoustical Society of America. 1992;91(3):1677–1689.

Dancer A, Grateau P, Cabanis A, Lejau J, Lafont D. Influence of the spacing of impulse noises (weapon noise) on the amplitude of the TTSs in man. J. Acoustique. 1991;4:421–434.

Dancer A, Grateau P, Cabanis A, Vaillant, T. Lafont D. Delayed temporary threshold shift induced by impulse noises (weapon noises) in men. Audiology. 1991;30:345–356.

Fedele P, Binseel M, Kalb J, Price GR. Using the auditory hazard assessment algorithm for humans (AHAAH) with hearing protection software, release MIL-STD-1474E. Aberdeen Proving Ground (MD); Army Research Laboratory (US): 2013 Dec. Report No.: ARL-TR-6748. Also available at http://www.arl.army.mil/www/default.cfm?technical_report=6945.

Guelke R, Keen JA. A study of the movements of the auditory ossicles under stroboscopic illumination. The Journal of Physiology. 1952;116(2):175–188.

Guinan JJ Jr, Peake WT. Middle-ear characteristics of anesthetized cats. The Journal of the Acoustical Society of America. 1967;41(5):1237–1261.

Hamernik RP, Ahroon WA, Hsueh KD. The energy spectrum of an impulse: its relation to hearing loss. The Journal of the Acoustical Society of America. 1991;90(1):197–204.

Hamery PJ, Dancer AL. Amplitude-sensitive attenuating earplugs. The Journal of the Acoustical Society of America. 1999;105(2):1130–1130

Henderson D, Hamernik RP. Impulse noise: critical review. The Journal of the Acoustical Society of America. 1986;80(2):569–584.

Ingard U, Ising H. Acoustic nonlinearity of an orifice. J. Acoust. Soc. Am. 1967;42(1):6–17. http://dx.doi.org/10.1121/1.1910576.

Johnson DL. Blast overpressure studies with animals and man: walk-up study. Fort Detrick, Frederick (MD): Army Medical Research and Development Command (US); 1993. Final Report Contract No. DAMD17-88-C-8141.

Kalb JT. An electroacoustic hearing protector simulator that accurately predicts pressure levels in the ear based on standard performance metrics. Aberdeen Proving Ground (MD): Human Research and Engineering Directorate; Army Research Laboratory (US); 2013 Aug. Report No. ARL-TR-6562. Also available at http://www.arl.army.mil/www/default.cfm?technical_report=6982.

Kalb JT. Hearing Protectors and hazard from impulse noise: melding methods and models. DoD Hearing Center of Excellence - CAVRN Working Group Meeting, 2015 Mar, San Diego, CA.

Kreyszig E. Advanced engineering mathematics. 3rd ed. New York (NY): John Wiley and Sons; 1972. p. 422.

Lutman ME, Martin AM. Development of an electroacoustic analogue model of the middle ear and acoustic reflex. Journal of Sound and Vibration. 1979;64(1):133–157.

Olsen HF. Dynamical analogies. New York (NY): D Van Nostrum Co; 1943.

Olsen HF. Acoustical engineering, Chapter IV. Princeton (NJ): D Van Nostrand Co, Inc; 1957.

Parmentier G, Dancer A, Buck K, Kronenberger G, Beck C. Artificial head (ATF) for evaluation of hearing protectors. Acta Acustica United with Acustica. 2000;86(5):847–852.

Patterson JH Jr, Gautier IM, Curd DL, Hamernik RP, Salvi RJ, Hargett CE Jr, Turrentine G. The role of peak pressure in determining the auditory hazard of impulse noise. Fort Rucker (AL): Army Aeromedical Research Laboratory (US); 1986 Apr. Report No.: 86-7.

Patterson JH Jr, Hamernik RP. An experimental basis for the estimation of auditory system hazard following exposure to impulse noise. Fort Rucker (AL): Army Aeromedical Research Laboratory (US); 1992. Report No.: ARL-92-17.

Patterson JH Jr, Hamernik RP, Hargett CE, Ahroon WA. An isohazard function for impulse noise. The Journal of the Acoustical Society of America. 1993;93(5):2860–2869.

Price GR. Loss of auditory sensitivity following exposure to spectrally narrow impulses. The Journal of the Acoustical Society of America. 1979;66(2):456–465.

Price GR. Validation of the auditory hazard assessment algorithm for the human with impulse noise data. J. Acoust. Soc. Am. 2007;122-5: 2786–2782. DOI: 10.1121/1.2785810.

Price GR. Implications of a critical level in the ear for assessment of noise hazard at high intensities. J. Acoust. Soc. Am. 1981;69:171.

Price GR. Relative hazard of weapons impulses. J. Acoust. Soc. Am. 1983;73:556.

Price GR, Kim HN, Lim DJ, Dunn D. Hazard from weapons impulses: histological and electrophysiological evidence. Aberdeen Proving Ground (MD): Army Research Laboratory (US); 1989. Report No.: HEL-TM-1-89.

Rayleigh L. The theory of sound. New York (NY): Dover Publications; 1945.

Shaw EAG, Thiessen GJ. Improved cushion for ear defenders. The Journal of the Acoustical Society of America. 1958;30(1):24–36.

Sivian LJ. Acoustic impedance of small orifices. The Journal of the Acoustical Society of America. 1935;7(2):94–101.

Zwislocki J. Ear protectors. In: Harris CM, editor. Handbook of Noise Control. New York (NY): McGraw-Hill; 1957. Chapter 8. p. 1–27.

List of Symbols, Abbreviations, and Acronyms

AHAAH	Auditory Hazard Assessment Algorithm for Humans
ANOR	allowed number of rounds
ARU	auditory risk unit
ATF	auditory test fixture
CAE	combat arms earplug
C-4	composition-4
dB	decibel
EACV	electro-acoustic component value
HPD	hearing protection device
HPM	Hearing Protector Module
IL	insertion loss
ISL	Institute at Saint-Louis
LDNL	level-dependent nonlinear
LIL	level-independent linear
MIATF	measurements in an acoustic test fixture
QRI	Quick Response Initiative
REAT	Real Ear Attenuation at Threshold
SPL	sound pressure level

1 (PDF) DEFENSE TECHNICAL INFORMATION CTR DTIC OCA

2 (PDF) DIRECTOR US ARMY RESEARCH LAB RDRL CIO LL IMAL HRA MAIL & RECORDS MGMT

1 (PDF) GOVT PRINTG OFC A MALHOTRA

1 (PDF) ARMY RSCH LABORATORY – HRED RDRL HRM D T DAVIS BLDG 5400 RM C242 REDSTONE ARSENAL AL 35898-7290

1 (PDF) ARMY RSCH LABORATOR HRED RDRL HRS EA DR V J RICE BLDG 4011 RM 217 1750 GREELEY RD FORT SAM HOUSTON TX 78234-5002

1 (PDF) ARMY RSCH LABORATORY – HRED RDRL HRM DG J RUBINSTEIN BLDG 333 PICATINNY ARSENAL NJ 07806-5000

1 (PDF) ARMY RSCH LABORATORY – HRED ARMC FIELD ELEMENT RDRL HRM CH C BURNS THIRD AVE BLDG 1467B RM 336 FORT KNOX KY 40121

1 (PDF) ARMY RSCH LABORATORY – HRED AWC FIELD ELEMENT RDRL HRM DJ D DURBIN BLDG 4506 (DCD) RM 107 FORT RUCKER AL 36362-5000

1 (PDF) ARMY RSCH LABORATORY – HRED RDRL HRM CK J REINHART 10125 KINGMAN RD BLDG 317 FORT BELVOIR VA 22060-5828

1 (PDF) ARMY RSCH LABORATORY – HRED RDRL HRM AY M BARNES 2520 HEALY AVE STE 1172 BLDG 51005 FORT HUACHUCA AZ 85613-7069

1 (PDF) ARMY RSCH LABORATORY – HRED RDRL HRM AP D UNGVARSKY POPE HALL BLDG 470 BCBL 806 HARRISON DR FORT LEAVENWORTH KS 66027-2302

1 (PDF) ARMY RSCH LABORATORY – HRED RDRL HRM AT J CHEN 12423 RESEARCH PKWY ORLANDO FL 32826-3276

1 (PDF) ARMY RSCH LAB – HRED HUMAN SYSTEMS INTEGRATION ENGR TACOM FIELD ELEMENT RDRL HRM CU P MUNYA 6501 E 11 MILE RD MS 284 BLDG 200A WARREN MI 48397-5000

1 (PDF) ARMY RSCH LABORATORY – HRED FIRES CTR OF EXCELLENCE FIELD ELEMENT RDRL HRM AF C HERNANDEZ 3040 NW AUSTIN RD RM 221 FORT SILL OK 73503-9043

1 (PDF) ARMY RSCH LABORATORY – HRED RDRL HRM AV W CULBERTSON 91012 STATION AVE FORT HOOD TX 76544-5073

1 (PDF) ARMY RSCH LABORATORY – HRED RDRL HRM DE A MARES 1733 PLEASONTON RD BOX 3 FORT BLISS TX 79916-6816

8 (PDF) ARMY RSCH LABORATORY – HRED
SIMULATION & TRAINING TECHNOLOGY CENTER
RDRL HRT COL G LAASE
RDRL HRT I MARTINEZ
RDRL HRT T R SOTTILARE
RDRL HRT B N FINKELSTEIN
RDRL HRT G A RODRIGUEZ
RDRL HRT I J HART
RDRL HRT M C METEVIER
RDRL HRT S B PETTIT
12423 RESEARCH PARKWAY
ORLANDO FL 32826

1 (PDF) ARMY RSCH LABORATORY – HRED
HQ USASOC
RDRL HRM CN R SPENCER
BLDG E2929 DESERT STORM DRIVE
FORT BRAGG NC 28310

1 (PDF) ARMY G1
DAPE MR B KNAPP
300 ARMY PENTAGON RM 2C489
WASHINGTON DC 20310-0300

ABERDEEN PROVING GROUND

12 (PDF) DIR USARL
RDRL HR
L ALLENDER
P FRANASZCZUK
K MCDOWELL
RDRL HRM
P SAVAGE-KNEPSHIELD
RDRL HRM AL
C PAULILLO
RDRL HRM B
J GRYNOVICKI
RDRL HRM C
L GARRETT
RDRL HRS
J LOCKETT
RDRL HRS B
M LAFIANDRA
RDRL HRS D
P FEDELE
A SCHARINE
RDRL HRS E
D HEADLEY

INTENTIONALLY LEFT BLANK.